

12-2004

Environment Assisted Cracking of Target Structural Materials Under Different Loading Conditions

Venkataramakrishnan Selvaraj
University of Nevada, Las Vegas

Follow this and additional works at: <https://digitalscholarship.unlv.edu/thesesdissertations>



Part of the [Mechanical Engineering Commons](#), [Metallurgy Commons](#), and the [Nuclear Engineering Commons](#)

Repository Citation

Selvaraj, Venkataramakrishnan, "Environment Assisted Cracking of Target Structural Materials Under Different Loading Conditions" (2004). *UNLV Theses, Dissertations, Professional Papers, and Capstones*. 1498.

<http://dx.doi.org/10.34917/3952688>

This Thesis is protected by copyright and/or related rights. It has been brought to you by Digital Scholarship@UNLV with permission from the rights-holder(s). You are free to use this Thesis in any way that is permitted by the copyright and related rights legislation that applies to your use. For other uses you need to obtain permission from the rights-holder(s) directly, unless additional rights are indicated by a Creative Commons license in the record and/or on the work itself.

This Thesis has been accepted for inclusion in UNLV Theses, Dissertations, Professional Papers, and Capstones by an authorized administrator of Digital Scholarship@UNLV. For more information, please contact digitalscholarship@unlv.edu.

ENVIRONMENT ASSISTED CRACKING OF TARGET STRUCTURAL
MATERIALS UNDER DIFFERENT LOADING CONDITIONS

by

Venkataramakrishnan Selvaraj

Bachelor of Engineering in Mechanical Engineering
University of Madras, Chennai, India
May 2002

A thesis submitted in partial fulfillment
of the requirements for the

Master of Science Degree in Mechanical Engineering
Department of Mechanical Engineering
Howard R. Hughes College of Engineering

Graduate College
University of Nevada, Las Vegas
December 2004

Thesis Approval Page

Provided by the Graduate College

ABSTRACT

Environment Assisted Cracking of Target Structural Materials under Different Loading Conditions

By

Venkataramakrishnan Selvaraj

Dr. Ajit K. Roy, Examination Committee Chair
Associate Professor, Mechanical Engineering
University of Nevada, Las Vegas

Martensitic Alloy HT-9 has been tested for its evaluation of stress corrosion cracking resistance in neutral and acidic solutions at ambient and elevated temperatures incorporating smooth and notched cylindrical specimens under constant load and slow strain rate (SSR) conditions. C-ring and U-bend specimens have also been tested for stress corrosion cracking evaluation in the acidic solution. The role of hydrogen on the cracking tendency has been evaluated by cathodic applied potential.

The results of constant load testing enabled the determination of the threshold stress for stress corrosion cracking in susceptible environments. The magnitudes of ductility parameters were reduced with increasing temperature. C-ring specimens showed cracking. Secondary cracks were observed by optical microscopy in specimens tested by the SSR technique. Fractographic evaluations by scanning electron microscopy revealed dimpled microstructure indicating ductile failure, and intergranular/transgranular brittle failures along the primary fracture face of the tested specimens.

TABLE OF CONTENTS

CHAPTER 1	INTRODUCTION	1
CHAPTER 2.	MATERIAL, TEST SPECIMENS AND ENVIRONMENTS	6
2.1	Test Material.....	6
2.2	Test Specimens	8
2.3	Test Environments	15
CHAPTER 3.	EXPERIMENTAL PROCEDURES.....	16
3.1	Tensile Testing.....	16
3.2	Constant-Load Testing	18
3.3	Slow-Strain-Rate Testing	20
3.4	Self-Load Testing.....	25
3.5	SCC Testing under Applied Potential.....	28
3.6	Surface Analyses.....	29
3.6.1	Optical Microscopy	30
3.6.2	Scanning Electron Microscopy	31
CHAPTER 4.	RESULTS	32
4.1	Constant-Load SCC Test.....	32
4.2	Slow-Strain Rate SCC Testing	36
4.3	SCC Testing using Self-Loaded Specimens.....	43
4.4	SCC Testing at controlled potential.....	47
4.5	Results of Micrograph Evaluation	48
4.5.1	Optical Microscopy	48
4.5.2	Scanning Electron Microscopy	50
CHAPTER 5.	DISCUSSION	53
5.1	Constant Load SCC testing	53
5.2	Slow Strain Rate SCC Testing.....	54
5.3	Self-Loaded SCC Testing.....	54
5.4	SCC testing under Econt	55
5.5	Microscopic Evaluation.....	55
CHAPTER 6.	SUMMARY AND CONCLUSION	57
CHAPTER 7.	FUTURE WORK	59
APPENDIX.	SLOW STRAIN DATA.....	60

BIBLIOGRAPHY.....	68
VITA.....	72

LIST OF TABLES

2.1 Thermal and Physical Properties of Alloy HT-9	7
2.2 Chemical Composition of Alloy HT-9 Tested	8
2.3 Chemical Compositions of Tested Solutions (gm/liter)	15
3.1 Ambient Temperature Mechanical Properties of Alloy HT-9	17
4.1 Results of CL SCC Tests using Smooth Specimens.....	33
4.2 Results of CL SCC Tests using Notched Specimens.....	35
4.3 SSR Test Results using Smooth Specimens.....	38
4.4 SSR Test results using Notched Specimens.....	40

LIST OF FIGURES

1.1 Overall Transmutation Process.....	2
1.2 Use of Neutrons during the Transmutation Process	2
2.1 Pictorial View of Smooth Specimen.....	10
2.2 Dimensions of Smooth Cylindrical Specimen	10
2.3 Pictorial View of Notched Cylindrical Specimens.....	11
2.4 Dimensions of Notched Cylindrical Specimen	11
2.5 Geometric Stress Concentration Factor for Notched Specimen.....	12
2.6 Pictorial View of C-Ring Specimen	13
2.7 Dimensions of C-ring Specimen	13
2.8 Pictorial view of U-bend specimen.....	14
2.9 Dimensions of U-Bend Specimen	14
3.1 MTS Setup	17
3.2 Constant-load Test Setup	19
3.3 A Typical Calibration Curve for a Proof Ring	20
3.4 CERT Machines for SSR Testing.....	21
3.5 SSR Test Setup	22
3.6 Load Frame Compliance Test	23
3.7 Figure for correction factor Z.....	26
3.8 Specimen Holder	27
3.9 Autoclave	28
3.10 Spot-Welded Cylindrical Specimen.....	28
3.11 SCC test Setup under E_{cont}	29
4.1 Applied Stress vs TTF for Smooth Specimen.....	34
4.2 Applied Stress vs TTF for Smooth Specimens	34
4.3 Applied Stress vs TTF for Notched specimen.....	36
4.4 Comparison of σ -e Diagrams using Smooth Specimens in Neutral Solution.....	37
4.5 Comparison of σ -e Diagrams using Smooth Specimens in Acidic Solution	37
4.6 Comparison of σ -e Diagrams using Notched Specimens in Neutral Solution.....	39
4.7 Comparison of σ -e Diagrams using Notched Specimens in Acidic Solution	39
4.8 Temperature vs Failure Stress	41
4.9 Temperature vs TTF	41
4.10 Temperature vs %EL	42
4.11 Temperature vs %RA.....	42
4.12 Appearances of C-Ring Specimens Tested in Acidic Solution.....	45
4.13 Appearances of U-Bend Specimen in Acidic Solution.....	46
4.14 Stress-Strain Diagrams with and without E_{cont}	47
4.15 Stress-Strain Diagrams with and without E_{cont}	48
4.16 Optical Micrograph of Alloy HT-9 after Quenching and Tempering	49
4.17 Secondary Cracks Determined by Optical Microscopy.....	49

4.18 Optical Micrograph of Failed C-Ring Specimen.....	50
4.19 SEM Micrographs of the Primary Fracture Face of Alloy HT-9	51
4.20 Intergranular Brittle Failure in C-Ring Specimen in 100°C Acidic Solution.....	52

ACKNOWLEDGMENTS

This work was performed under the able guidance of my advisor, Dr. Ajit K. Roy. It was my privilege and pleasure to work with him on this project and I would like to express my gratitude to him for his invaluable contributions.

I would like to thank Dr. Anthony E. Hechanova, Dr. Brendan J. O'Toole and Dr. Rama Venkat, for their valuable suggestions and support throughout this investigation.

I would like to acknowledge the assistance offered by my associates in the Materials Performance Laboratory. I would also like to express my appreciation to my parents for their sacrifices, persistent support and boundless confidence in me.

Finally, I would like to acknowledge the United States Department of Energy for the financial Support.

CHAPTER 1

INTRODUCTION

The Yucca Mountain site near Las Vegas, Nevada has recently been proposed to be the nation's geologic repository to contain spent-nuclear-fuel (SNF) and defense high-level-radioactive waste (HLW) for an extensive time period. Such a long disposal period is designed to ensure a reduction in the radioactivity of these nuclear wastes by virtue of their natural decay so that the ground water underneath this repository does not get contaminated in course of time. However, with time, more radioactive waste will be generated from the existing nuclear power plants thus, requiring their disposal at either the proposed Yucca Mountain site or repositories to be built in the future.

In order to circumvent the problems associated with the disposal of highly radioactive nuclear waste, the United States Department of Energy (USDOE) has recently initiated an extensive effort to develop an alternate method to reduce the radioactivity of HLW/SNF, and subsequently dispose of them. This method, known as transmutation, is based on the reduction or elimination of radioactive species and isotopes from HLW/SNF by bombarding them with proton-generated neutrons, followed by their disposal in the proposed geologic repository.^[1] These neutrons are generated by impinging protons from an accelerator or a reactor onto a target material such as molten lead-bismuth-eutectic (LBE). The transmutation process is illustrated in Figures 1.1 and 1.2. The molten LBE

will be contained in a structural vessel made of a suitable material such as martensitic Alloy EP-823 or Alloy HT-9.

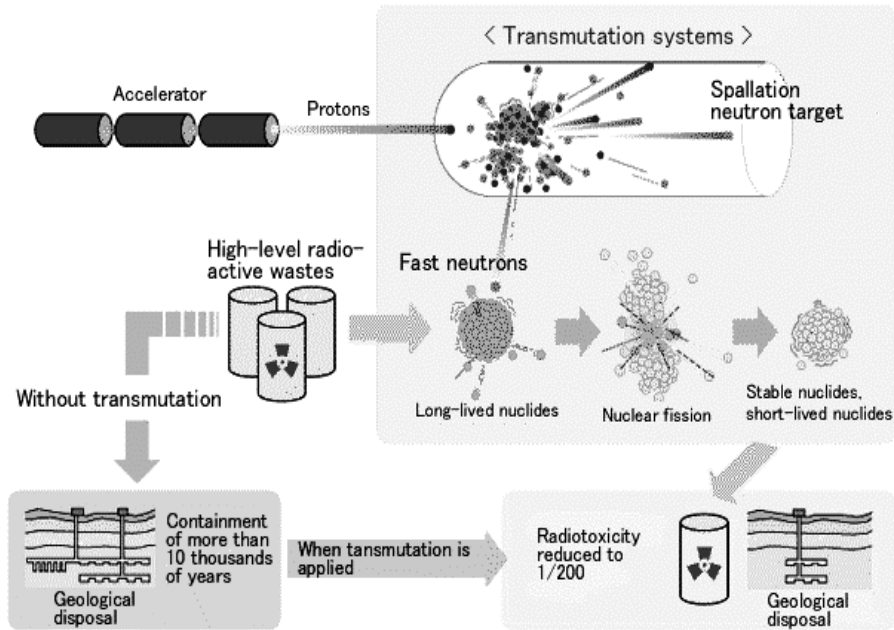


Figure 1.1 Overall Transmutation Process

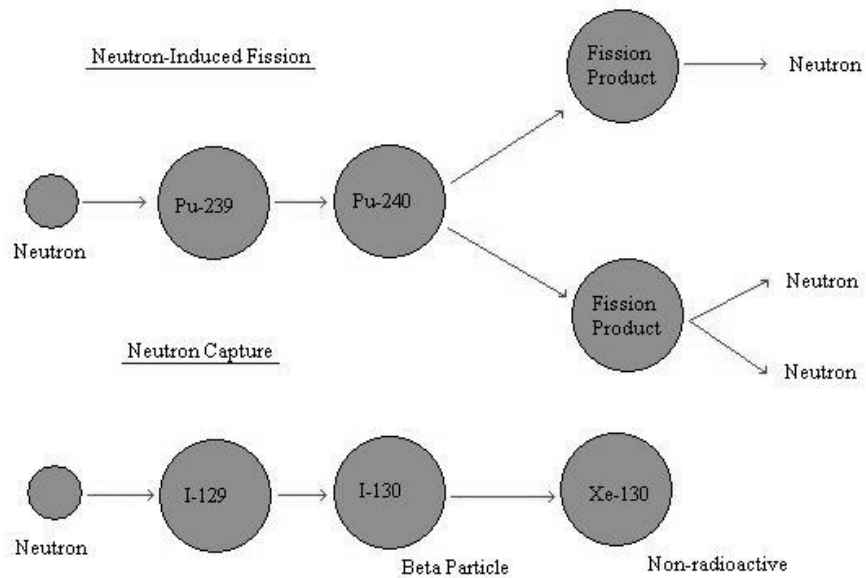


Figure 1.2 Use of Neutrons during the Transmutation Process

During the transmutation process, hydrogen and helium can be generated, which may cause degradation to the target structural material. Further, since the target material will be subjected to stresses during the generation of neutrons, high stresses may also be generated in the structural material causing it to suffer from environment-induced degradation such as liquid-metal-embrittlement, stress corrosion cracking (SCC) and hydrogen-embrittlement (HE).^[2,3]

Molten LBE is a very effective nuclear coolant because of its low melting temperature, low vapor pressure, good neutron yield, low neutron absorption, high boiling temperature, high atomic number and good heat removal capability.^[4] The Russians have developed an extensive knowledge on LBE by virtue of its use as a coolant in their alpha-class submarines. Further, LBE has been identified to be an efficient spallation target source during the transmutation process.

The anticipated cracking to be experienced by the structural material in the presence of molten LBE is commonly known as liquid-metal-embrittlement,^[5] which is a result of the reduction in cohesive strength of the structural metal surface due to its interaction with the molten metal. On the other hand, degradations such as SCC and HE are related to electrochemical mechanisms involving anodic and cathodic reactions while exposed to aggressive aqueous environments in a stressed condition.^[6] Thus, the mechanism of cracking in the presence of molten LBE is somewhat different from that in the presence of aqueous environments.

SCC is an environment-assisted embrittlement of a metallic material or an alloy resulting from the combined effect of a corrosive environment and a tensile stress. The stress may result from applied forces or locked-in residual stresses. Only specific

combinations of alloy and chemical environment can lead to SCC. Usually, SCC begins with the rupturing of the protective oxide film on the metal surface by either mechanical means or by the action of chemical species, such as chloride ions. The cracks resulting from SCC may be either ductile or brittle or a combination of both. Cracking may also be intergranular, transgranular, or a combination of both depending on the alloy, its metallurgical microstructure, and the environment. As stated earlier, hydrogen and helium produced during nuclear reactions can segregate to vacancy clusters and internal voids, thus, leading to HE in the target structural material. ^[7]

The HE process may depend on two major factors: (1) the presence of hydrogen; (2) the transport processes involved in moving hydrogen from its source to the locations where it reacts with the metal to cause embrittlement. Body-centered-cubic (BCC) metals are most susceptible to HE. ^[8] The primary characteristics of HE are its strain-rate sensitivity, temperature-dependence and susceptibility to delayed-failure. In addition to embrittlement, localized corrosion may also occur in the structural material, which is a degradation mode in which an intense attack takes place at localized sites on the surface of the material, while the rest corrodes at a lower rate.

Since the target structural material may become susceptible to liquid-metal-embrittlement in the presence of molten LBE, SCC testing using self-loaded specimens of martensitic stainless steels was planned to be initiated at the Los Alamos National Laboratory (LANL) using its LBE loop. In parallel, SCC/HE tests were also initiated at UNLV in aqueous environments of different pH values to develop baseline corrosion data on similar target structural materials. Even though, a direct comparison of degradation in molten LBE and aqueous environments may be difficult due to the differences in the

degradation mechanism, it is appropriate to assume that at least some comparisons can be made as to the surface characteristics of the tested material due to its exposure in either of these environments.

SCC testing using self-loaded specimens could not be accommodated in molten LBE at LANL due to some technical difficulties. Therefore, efforts are ongoing to develop a test facility at UNLV to accommodate corrosion testing in the presence of molten LBE. While this facility is being developed, an extensive corrosion research program was initiated at UNLV to evaluate environment-induced degradations in martensitic structural materials in the presence of aqueous environments of difficult pH values at ambient and elevated temperatures incorporating numerous state-of-the-art testing techniques.

This thesis is focused on presenting and analyzing the results of SCC and HE experiments of Alloy HT-9 using constant-load, slow-strain-rate (SSR) and self-loaded testing techniques. The susceptibility to HE has been determined by applying controlled cathodic potential while the specimen was loaded in tension. The metallographic and fractographic evaluations of the broken specimens were conducted by optical microscopy and scanning electron microscopy, respectively.

Detailed discussions on the metallurgical characterization of Alloy HT-9, test specimen configurations, environments and experimental techniques used are presented in subsequent sections. Further, the resultant data, their analyses and viable discussions have been presented. Based on the analysis of overall data and their discussion, plausible explanations on degradation mechanisms have also been attempted.

CHAPTER 2

MATERIAL, TEST SPECIMENS AND ENVIRONMENTS

2.1. Test Material

Martensitic stainless steels are currently finding extensive applications in nuclear reactors as substitutes for austenitic steels. ^[9] They are basically alloys of carbon (C) and chromium (Cr) having body-centered-cubic (BCC) or body-centered-tetragonal (BCT) crystal structure in the hardened state. They are ferromagnetic and hardenable by heat-treatments. Martensitic stainless steels are usually preferred for their relatively high strength, moderate resistance to corrosion, and good fatigue properties following suitable thermal treatments. The Cr content of these materials normally ranges between 9 to 18 wt%, and their C content can be as high as 1.2 wt%. The composition of Cr and C are balanced to ensure a martensitic micro structure after hardening. Molybdenum (Mo) and nickel (Ni) can also be added to improve the mechanical properties or the corrosion resistance. When higher Cr levels are used to improve corrosion resistance, the presence of Ni can also help in maintaining the desired microstructure and prevent the formation of excessive free-ferrite. ^[10]

Since the as-hardened martensitic structure is quite brittle, this material is typically reheated at lower temperatures to relieve the internal stresses within the microstructure or reheated to slightly higher temperatures to soften (temper) the material to intermediate hardness levels. Two martensitic alloys are of great interest for nuclear applications. They

are Alloys HT-9 and T-91, both of which contain Cr and Mo. These alloys have been extensively used in Europe as target structural material in the transmutation systems as well as for the internal components in the U.S. experimental liquid metal fast breeder reactors (LMFBR) due to their moderate corrosion resistance, optimum strength, the ease of manufacturing, and relatively lower cost. ^[11] Alloy HT-9 is a Swedish nuclear grade martensitic iron-nickel-chromium-molybdenum (Fe-Ni-Cr-Mo) stainless steel. T-91 falls within an ASTM designation ^[12] having Cr, Mo, Nb and V in it.

Alloy HT-9 was specifically developed for high temperature applications, where the corrosion-resistance inherent in austenitic stainless steels is not required. It has good swelling resistance and is also resistant to irradiation embrittlement, particularly at 60°C. It has been an excellent material for cladding and duct applications in liquid-metal reactors. The thermal and physical properties of Alloy HT-9 are shown in Table 2.1. ^[13]

Table 2.1 Thermal and Physical Properties of Alloy HT-9

Thermal Conductivity, W / m * K	28
Modulus of Elasticity, GPa (106 psi)	160
Poisson's Ratio	0.33
Coefficient of Thermal Expansion per °C (°F) * 10-6	12.5

Alloy HT-9 also possesses the following properties

- Lower coefficient of thermal expansion and high thermal conductivity than austenitic steels
- High swelling resistance in fast neutron, ion and electron irradiation conditions
- High creep strength
- Higher Cr corrosion rates than austenitic/Ni based alloys

- Addition of Cu may cause irradiation embrittlement

Experimental heats of Alloy HT-9 were melted at the Timken Research Laboratory, Ohio, by a vacuum-induction-melting practice followed by processes that included forging and hot rolling. These hot rolled products were subsequently cold rolled to produce round bars of different sizes. These cold-rolled bars were initially austenitized at 1010°C followed by oil-quenching. Hard but brittle martensitic microstructures were developed in these bars due to austenitizing and quenching. Therefore, tempering operations were performed at 621°C to produce fine-grained and fully-tempered martensitic microstructures without the formation of any retained austenite, thus producing appreciable ductility. The chemical composition of Alloy HT-9 tested in this study is given in Table 2.2.

Table 2.2 Chemical Composition of Alloy HT-9 Tested

Material	Elements (wt %)-balance of composition is Fe													
	C	Mn	P	S	Si	Cr	Ni	Mo	Cu	V	W	Cb	B	Ce
Alloy HT-9	.18	.4	.012	.2	0.2	12.26	0.49	1	.01	.3	.46	--	--	--

2.2. Test Specimens

The following types of specimens were used for SCC evaluation

1. Tensile Specimens
 - a. Smooth Tensile
 - b. Notched Tensile

2. Self Loaded Specimens

- a. C-ring
- b. U-bend

Cylindrical smooth and notched specimens (4-inch overall length, 1-inch gage length and 0.25-inch gage diameter) of Alloy HT-9 were machined from the heat-treated bars in such a way that the gage section was parallel to the longitudinal rolling direction. It is known that imperfections such as notch or dents can be present in machined specimens, which can influence the performance of the material. In view of this rationale, a V-shaped notch of 0.156-inch diameter, with an angle of 60° and a maximum depth of 0.05 inch around the gage diameter was added to the center of the gage section of the test specimen to study the effect of stress concentration. A gage length to gage diameter (l/d) ratio of 4 was maintained for both smooth and notched specimens according to the ASTM Designation E 8. ^[14] The Dimensions for the specimens are chosen from the prior works performed in material performance laboratory in UNLV. Pictorial views and detailed dimensions of smooth and notched cylindrical specimen are shown in Figures 2.1 through 2.4.



Figure 2.1 Pictorial View of Smooth Specimen

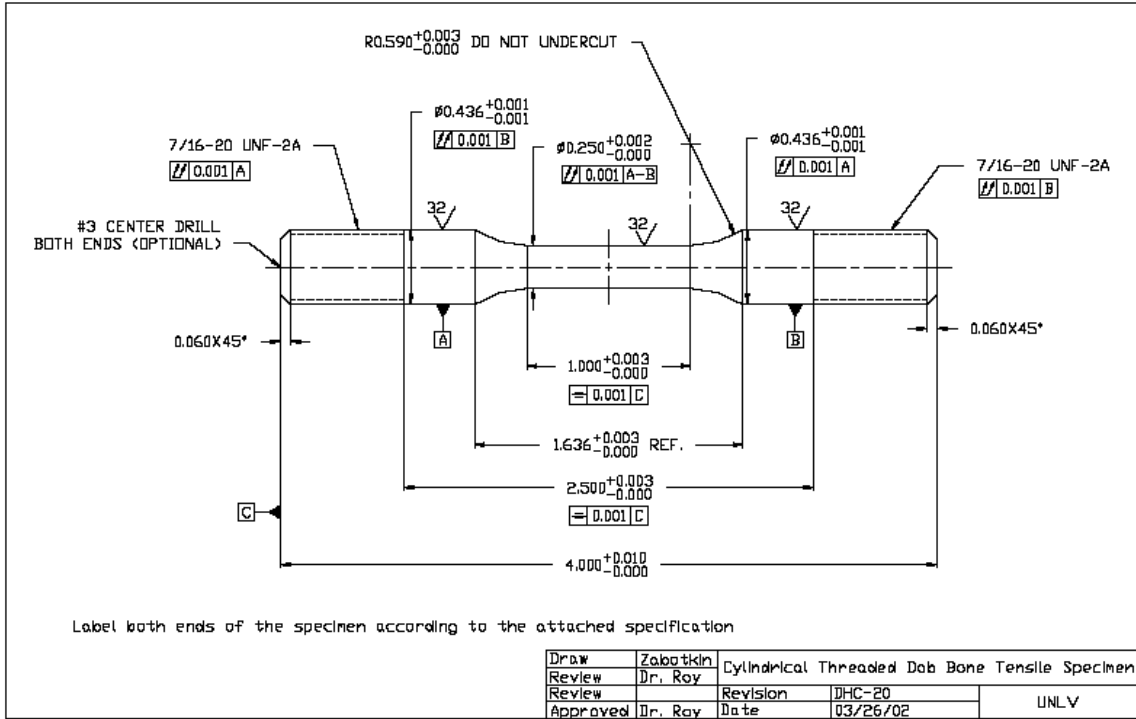


Figure 2.2 Dimensions of Smooth Cylindrical Specimen



Figure 2.3 Pictorial View of Notched Cylindrical Specimen

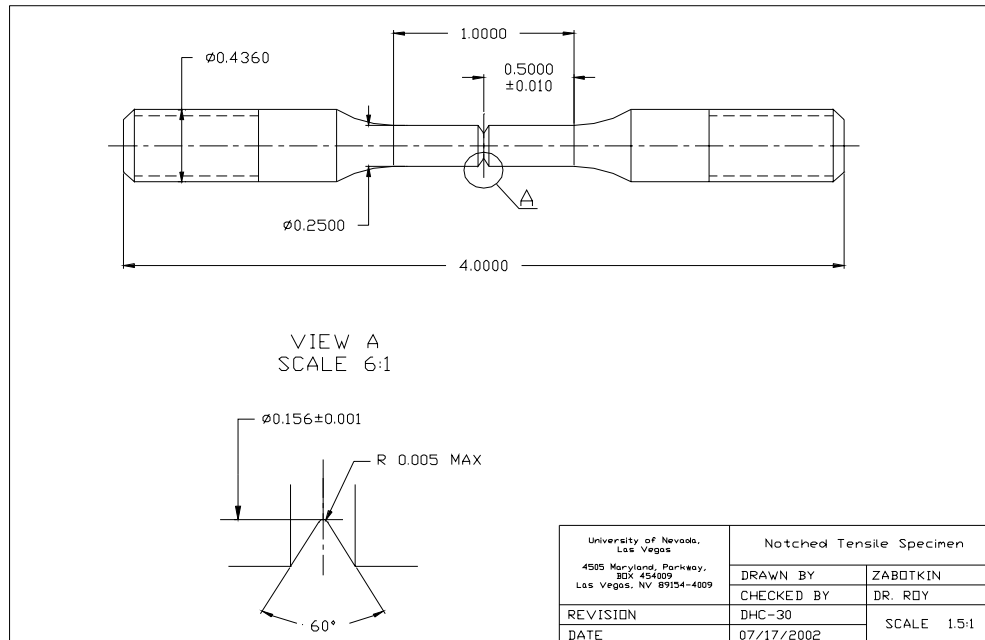


Figure 2.4 Dimensions of Notched Cylindrical Specimen

The ratios of D/d and r/d were used to estimate the magnitude of the stress concentration factor (k_t)^[15] based on the plot shown in Figure 2.5. An approximate k_t value of 1.45 was determined based on the following analysis.

$$\frac{D}{d} = \frac{0.250in}{0.156in} = 1.60$$

$$\frac{r}{d} = \frac{0.05}{0.156} = 0.32$$

Where,

D = Gage diameter of the specimen

d = Notch diameter of the specimen

r = Radius of curvature at the root of the notch

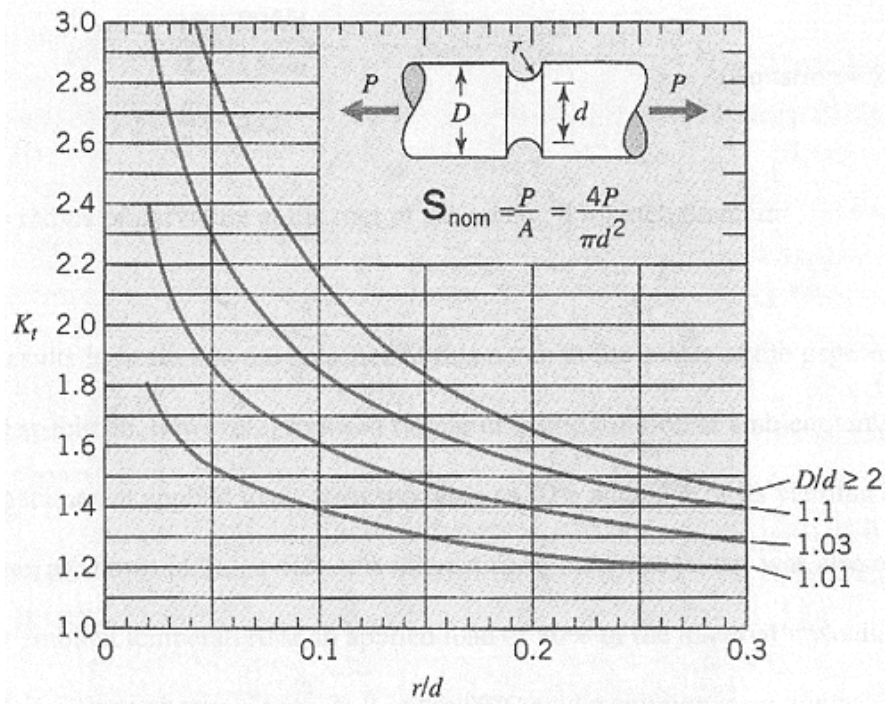


Figure 2.5 Geometric Stress Concentration Factor for Notched Specimen^[15]

Self-loaded specimens such as C-ring and U-bend (Figures 2.6 - 2.9) were also used in this investigation for the evaluation of SCC. The C-ring is a versatile and economic type of specimen for quantitatively determining the susceptibility of a material to SCC of all types of alloys in a wide variety of product forms. It is particularly suitable for making short-transverse tests of various products. The U-bend specimen is generally a rectangular strip which is bent 180° around a predetermined radius and maintained in this

constant strain condition during the SCC testing. The sizes of C-rings may be varied over a wide range, but the use of C-rings with an outside diameter less than about 16 mm are not recommended because of increased difficulties in machining and decreased precision in stressing.

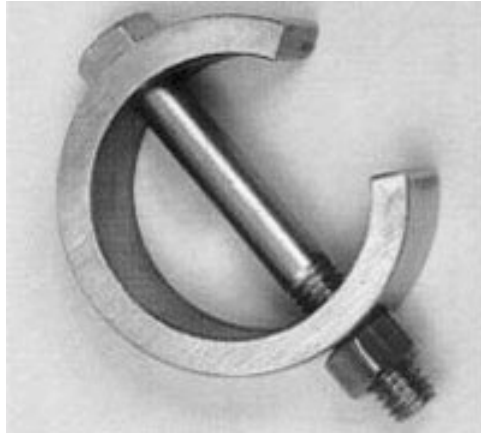


Figure 2.6 Pictorial View of C-ring Specimen

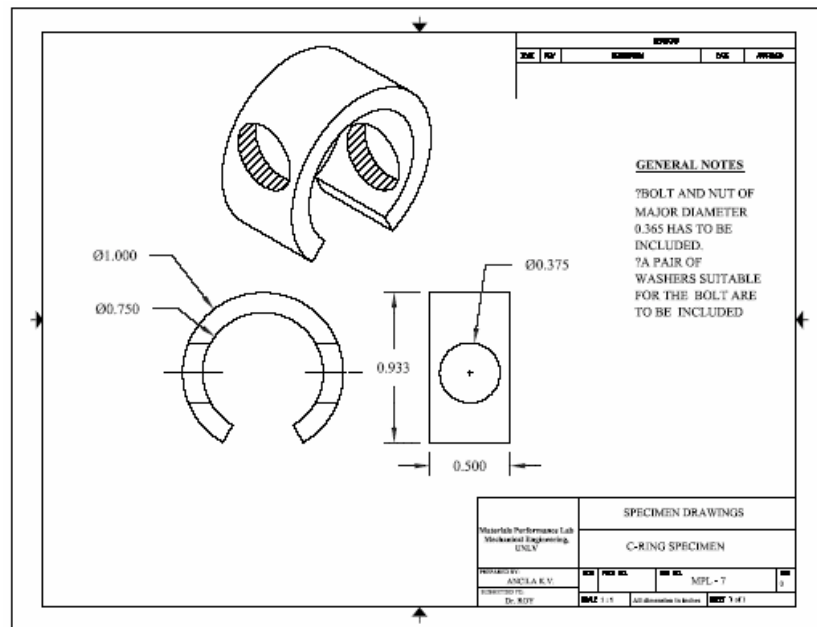


Figure 2.7 Dimensions of C-ring Specimen



Figure 2.8 Pictorial View of U-bend Specimen

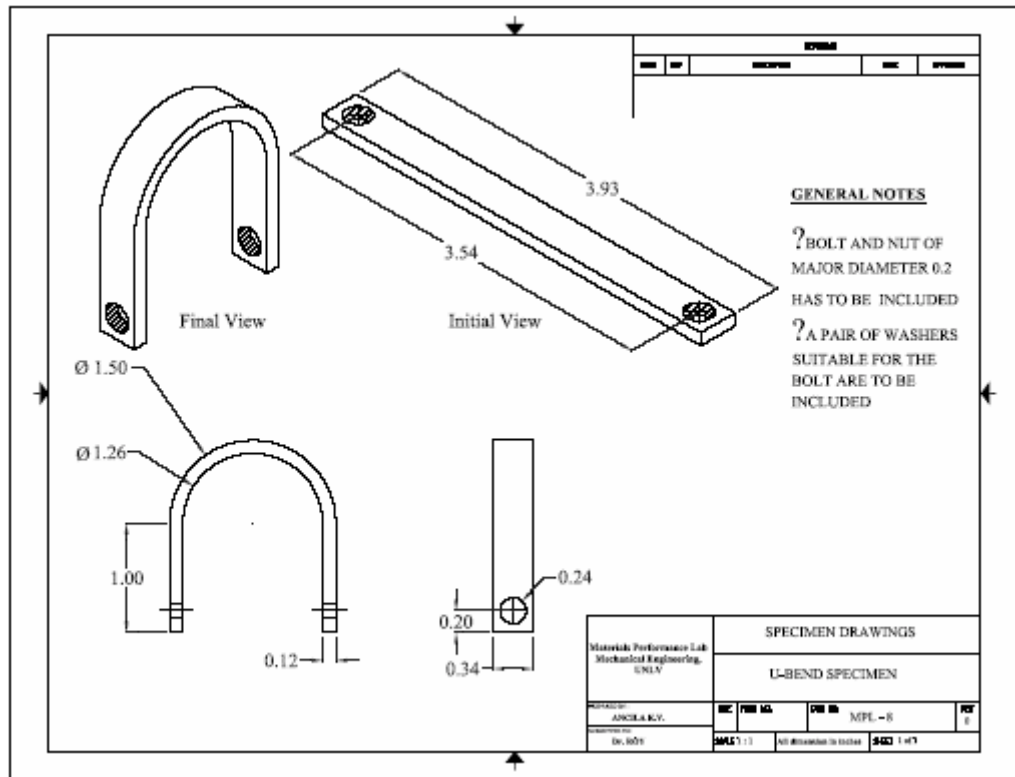


Figure 2.9 Dimensions of U-bend Specimen

2.3. Test Environments

Since the molten LBE could have a tendency to degrade the structural material by corrosion and embrittlement, SCC testing using C-ring and U-bend specimens were planned at LANL using its LBE loop. However, this testing could not be performed due to some technical difficulties. Therefore, efforts are ongoing to develop a test facility at UNLV to accommodate corrosion testing in the presence of molten LBE.

While this facility is being developed, a corrosion research program was initiated at UNLV to evaluate environment-induced degradations in Alloy HT-9 in aqueous environments of different pH values at ambient and elevated temperatures using tensile, C-ring and U-bend specimens. The compositions of these aqueous environments are given in Table 2.4.

Table 2.3 Chemical Compositions of Tested Solutions (gm/liter)

Environment(pH)	CaCl ₂	K ₂ SO ₄	MgSO ₄	NaCl	NaNO ₃	Na ₂ SO ₄
Neutral (6.0-6.5)	2.77	7.58	4.95	39.97	31.53	56.74
Acidic (2.0-2.2)	Same as above except for an addition of HCl to adjust the pH to the desired range					

CHAPTER 3

EXPERIMENTAL PROCEDURES

The ambient-temperature mechanical properties of Alloy HT-9 were determined by using a materials testing system (MTS) equipment. The susceptibility of this alloy to SCC in acidic and neutral environments was evaluated by using constant-load (CL), slow-strain-rate (SSR) and self-load testing techniques at temperatures ranging from ambient to 100°C. The effect of hydrogen on the cracking behavior of Alloy HT-9 was determined by applying cathodic (negative) electrochemical potential, while the specimen was strained in tension in the aqueous solution. Further, optical microscopy and SEM were used for the metallographic and fractographic evaluations, respectively.

3.1. Tensile Testing

An axial/torsional servohydraulic and computer-controlled MTS unit was used to determine the tensile properties including yield strength (YS), ultimate tensile strength (UTS), and ductility parameters such as percentage elongation (%El) and percentage reduction in area (%RA) at ambient temperature and at atmospheric conditions according to the ASTM designation E 8. ^[14] The MTS test setup is shown in Figure 3.1. The ambient temperature tensile properties of Alloy HT-9 obtained by using the MTS machine at a strain rate of 10^{-3} second are given in Table 3.1.

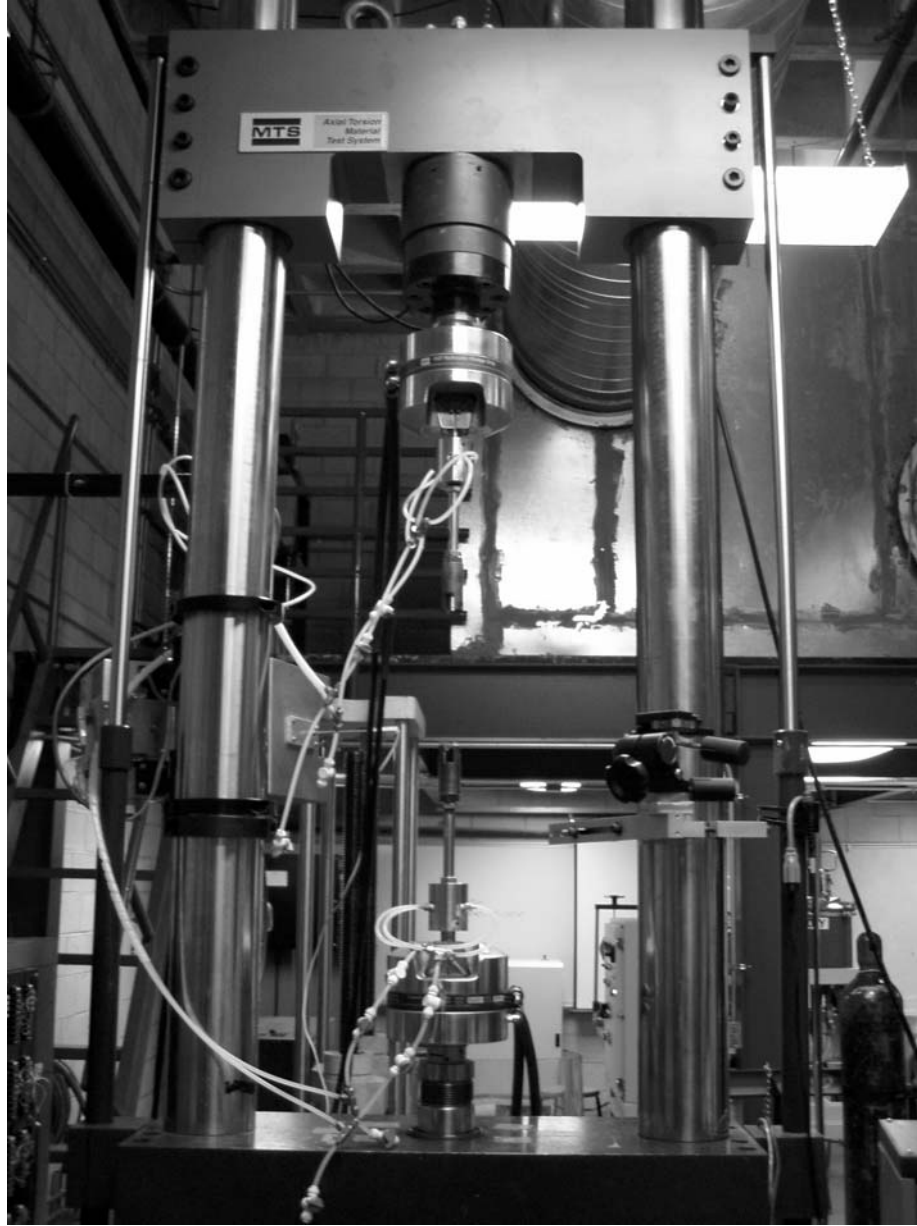


Figure 3.1 MTS Setup

Table 3.1 Ambient Temperature Mechanical Properties of Alloy HT-9

Material/Heat No.	YS (ksi)	UTS (ksi)	%El	%RA
Alloy HT-9/2048	118	139	22.1	62.3

3.2. Constant-Load Testing

A calibrated proof ring was used for testing at constant load (CL). These proof-rings were specifically designed to meet a National Association of Corrosion Engineers (NACE) standard. ^[16] Each individually calibrated proof ring was made by Cortest Inc using precision-mechanics alloy steel and was accompanied by a calibration curve showing the load versus deflection. The test specimens were loaded under uniaxial tension. The ring deflection was measured with a 8-9" diameter micrometer, with the supplied dial indicator. The tensile load on the proof ring was quickly and easily adjusted using a standard wrench on the tension-adjusting screw and lock nut. A thrust bearing distributed the load and prevented seizure. The specimen grips in these proof rings were made of stainless steel, fully-resistant to corrosion in the testing environments. The environmental test chamber was secured by O-ring seals that prevented any leakage during testing. The environmental chambers made of highly corrosion-resistant Hasteloy C-276 were used for testing at elevated temperatures. The experimental setup is shown in Figure 3.2

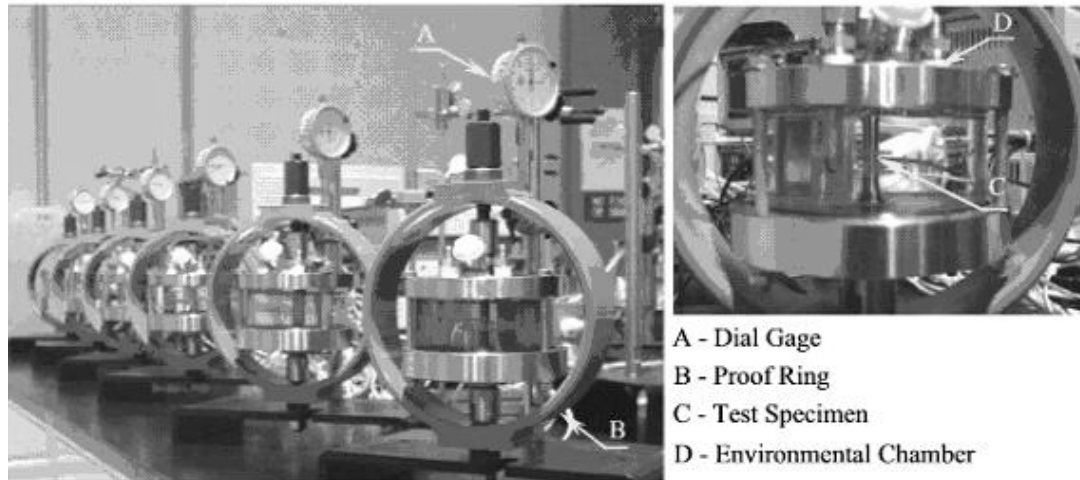


Figure 3.2 Constant-Load Test Setup

The amount of deflection needed to apply the desired load in the CL testing was determined by use of the calibration curve of each proof ring, as shown in Figure 3.3. The magnitude of the applied stress was based on the ambient-temperature tensile YS of the test materials. The specimens were loaded at stress values equivalent to different percentages of the material's YS value, and the corresponding time-to-failure (TTF) was recorded. The determination of the SCC tendency using this technique was based on the TTF for the maximum test duration of 30 days. An automatic timer attached to the test specimen recorded the TTF. The cracking susceptibility was expressed in terms of a threshold stress (σ_{th}) for SCC below which cracking did not occur during the maximum test duration of 30 days.

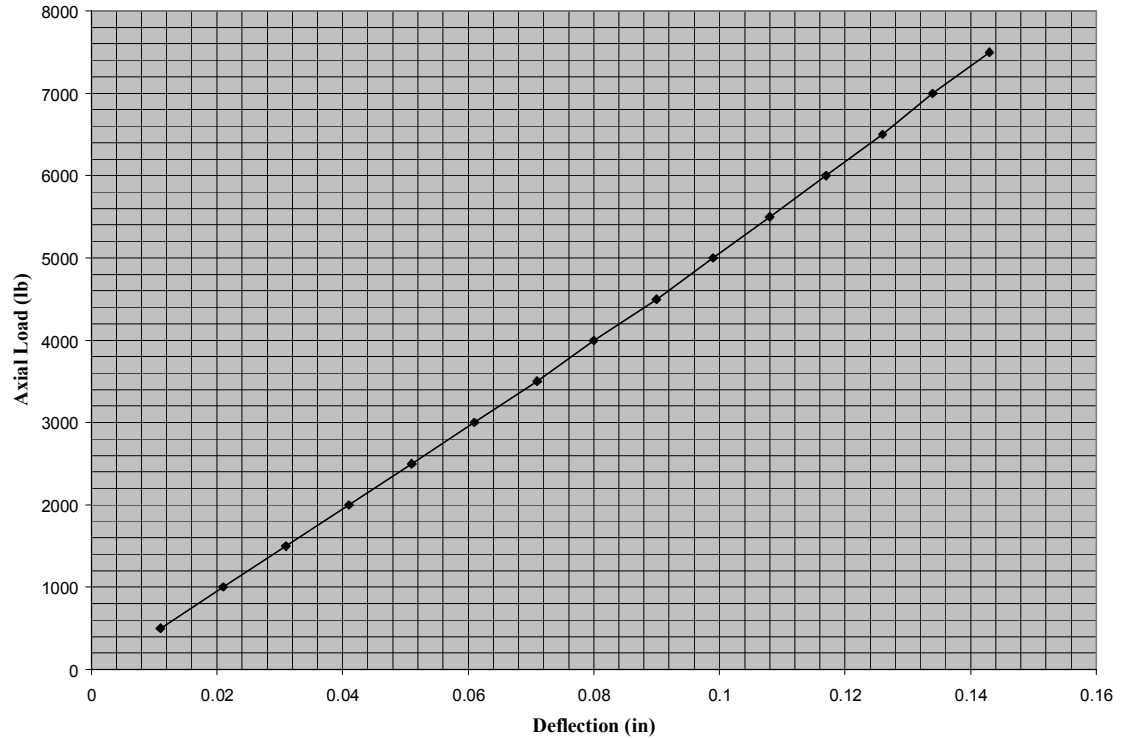


Figure 3.3 A Typical Calibration Curve for a Proof Ring

3.3. Slow-Strain-Rate Testing

During the late 1960s, a dynamic SCC evaluation technique had emerged, which is known as constant-strain-rate or slow-strain-rate testing (SSR) technique. SSR testing used in this investigation was performed in a specially-designed system known as a constant-extension-rate-testing (CERT) machine, shown in Figure 3.4. This equipment allowed testing to simulate a broad range of load, temperature, pressure, strain-rate and environmental conditions using both mechanical and electrochemical corrosion testing techniques. These machines, designed and manufactured by Cortest Inc., offered accuracy and flexibility in testing the effects of strain rate, providing up to 7500 lbs of load capacity with linear extension rates ranging from 10^{-5} to 10^{-8} in/sec.

To ensure the maximum accuracy in test results, this apparatus was comprised of a heavy-duty load-frame that minimized the system compliance while maintaining precise axial alignment of the load train. An all-gear drive system provided consistent extension rate. This machine provided the maximum flexibility and working space for test sample configuration, environmental chamber design, and accessibility. An added feature included in this model (model# 3451) for ease of operation was a quick-hand wheel to apply a pre-load prior to the operation.

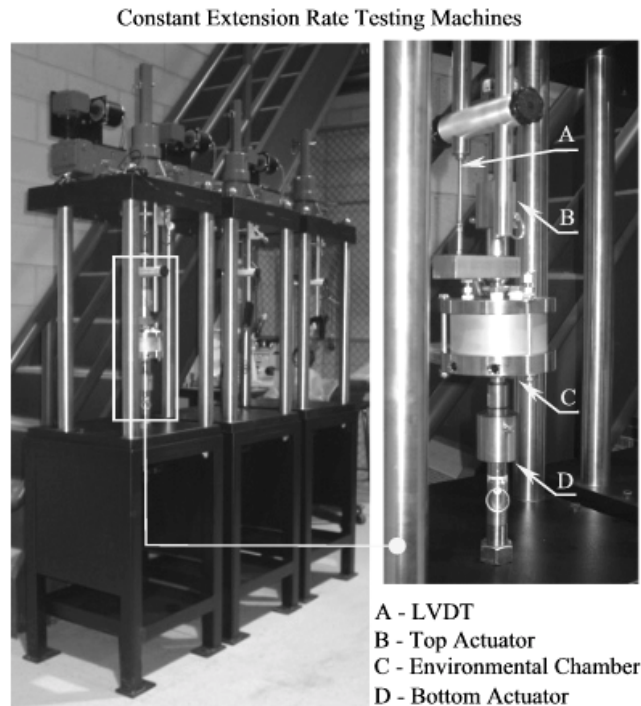


Figure 3.4 CERT Machines for SSR Testing

The SSR test setup used in this study consisted of a top-loaded actuator, testing chamber, linear variable differential transducer (LVDT) and load cell, as shown in Figure 3.5. The top-loaded actuator was intended to pull the specimen at a specified strain rate

so that the spilled solution, if any, would not damage the actuator. A heating cartridge was connected to the bottom cover of the environmental chamber for elevated-temperature testing. A thermocouple was connected on the top cover of this chamber to monitor the inside temperature. The load cell was intended to measure the applied load through an interface with the front panel user interface. The LVDT was used to record the displacement of the gage section during the SSR testing.

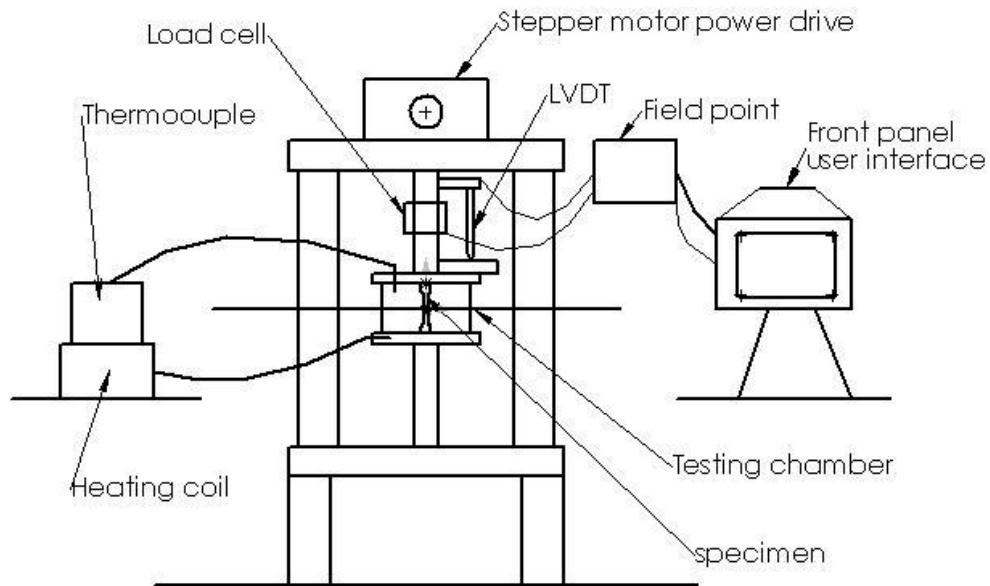


Figure 3.5 SSR Test Setup

Prior to the performance of SCC testing by the SSR technique, the load-frame-compliance factor (LFCF- the deflection in the frame per unit load), was determined by using a Type 430 ferritic stainless steel specimen. The generated LFCF data are shown in Figure 3.6. These LFCF values were inputted to a load frame acquisition system prior to the SCC testing. The resultant LFCF values are also shown in Figure 3.6.

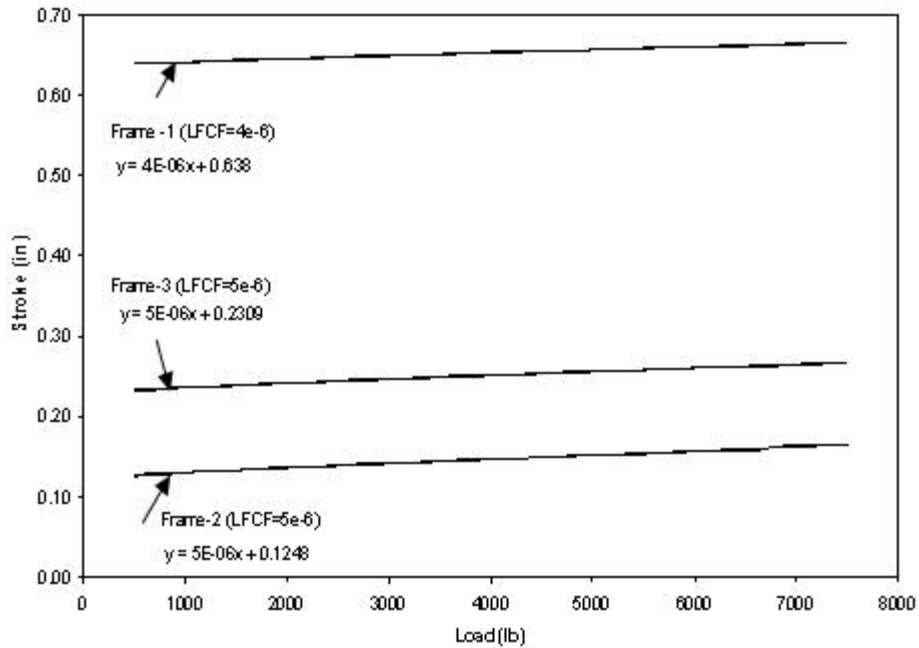


Figure 3.6 Load Frame Compliance Test

A strain rate of 3.3×10^{-6} was used during the SSR testing. This strain rate was selected based upon prior research work performed at the Lawrence Livermore National Laboratory (LLNL).^[17] It is well known that the SCC occurrence is an effect of two significant factors such as the applied/residual stress and a susceptible environment. If the stress is applied at a very fast rate to the test specimen, while it is exposed to the aqueous environment, the resultant failure may not be different from the conventional mechanical deformation produced without an environment. On the other hand, if the strain rate is too slow, the resultant failure may simply be attributed to the corrosion damage due to the environmental interaction with the material, thus, causing breakdown of the protective surface film. In view of this rationale, the SSR testing at LLNL was initially conducted at

strain rates ranging between 10^{-5} and 10^{-7} . Based upon the experimental work at LLNL, it was determined that a strain rate of around 10^{-6} would provide the most effective contributions of both the mechanical and environmental factors in enhancing the environment-induced cracking susceptibility during the SSR testing.

During SCC testing by the SSR method, the specimen was continuously strained in tension until fracture, in contrast to more conventional SCC tests conducted under sustained loading conditions. The application of a slow dynamic straining during the SSR testing to the specimen caused failure that probably might not occur under a constant load or might have taken a prohibitively longer duration to initiate cracks in producing failures in the tested specimens.

Load versus displacement, and stress versus strain curves were plotted during these tests. Dimensions (length and diameter) of the test specimens were measured before and after testing. The cracking tendency in the SSR tests was characterized by the TTF, and a number of ductility parameters such as %El and the %RA. Further, the maximum stress (σ_m), and the true failure stress (σ_f) obtained from the stress-strain diagram and the final dimensions were used. The magnitudes of %El, %RA, σ_m and σ_f were calculated using the following equations:

$$\% \text{ El} = \left(\frac{L_f - L_o}{L_o} \right) \times 100 ; L_f > L_o \quad (\text{Equation 3.1})$$

$$\% \text{ RA} = \left(\frac{A_o - A_f}{A_o} \right) \times 100 ; A_o > A_f \quad (\text{Equation 3.2})$$

$$\sigma_f = \frac{P_f}{A_f} \quad (\text{Equation 3.3})$$

$$\sigma_m = \frac{P_m}{A_m} \quad (\text{Equation 3.4})$$

$$A = \frac{\pi \times D^2}{4} \quad (\text{Equation 3.5})$$

Where,

A_0 = Initial cross sectional area

A_m = Cross sectional area at maximum load

A_f = Final cross sectional area at failure

P_m = Ultimate tensile load

P_f = Failure load

L_0 = Initial length

L_f = Final length

3.4. Self-Load Testing

The susceptibility of Alloy HT-9 to SCC in the test solution using C-ring and U-bend specimen was evaluated according to the ASTM designation G38-01^[18] and G 30-97^[19] respectively. The magnitude of the outer diameter of the C-ring specimen corresponding to the desired percentage of the material YS was calculated using an equation shown below. The C-ring specimen was stressed by tightening the bolt and the nut until the final outer diameter was reached.

In case of the U-bend specimens, the applied stress was varied with different deflections of two legs from the original position. A line was marked at a constant distance from the end of the leg. The distance between the two legs in the marked point is measured. This difference in distance between the two legs at the marked point is varied for various applied stresses.

The loaded specimens were then immersed inside an Acidic solution either in a desiccator or in an autoclave for testing at the room and elevated temperatures, respectively. The test specimens were periodically removed from the test cells for visual and microscopic evaluation. Some of the specimens were returned to test cells for further exposure if no cracks were observed. The picture of the specimen holder and the Autoclave is shown in Figures 3.8 and 3.9, respectively.



Figure 3.8 Specimen Holder

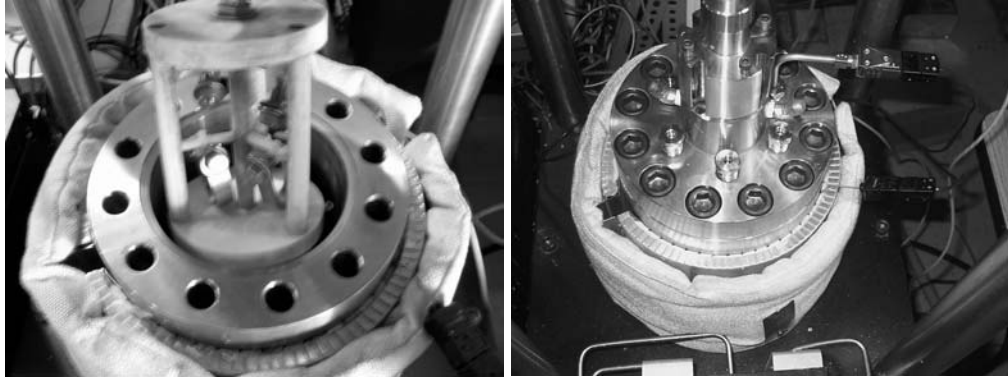


Figure 3.9 Self-Loaded Testing Setup

3.5. SCC Testing under Applied Potential

A limited number of SCC tests were performed in the acidic solution using the SSR technique at controlled cathodic potential (E_{cont}) to study the effect of hydrogen on the cracking susceptibility of Alloy HT-9. The magnitude of E_{cont} was based on the corrosion potential (E_{corr}) of this material performed in a similar environment by a previous investigator. ^[20] The Spot-Welded Cylindrical Specimen is shown in Figure 3.10 and the SCC test setup under E_{cont} is illustrated in Figure 3.11, showing the application of the applied potential by use of a conductive wire, spot-welded to the tensile specimen at the shoulder.

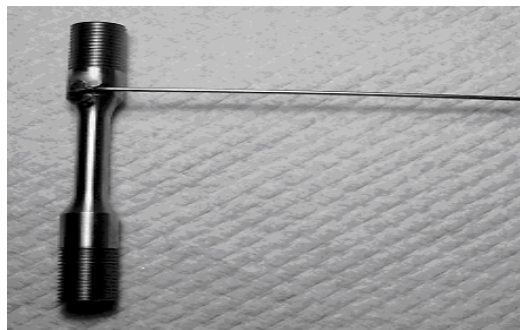


Figure 3.10 Spot-Welded Cylindrical Specimen

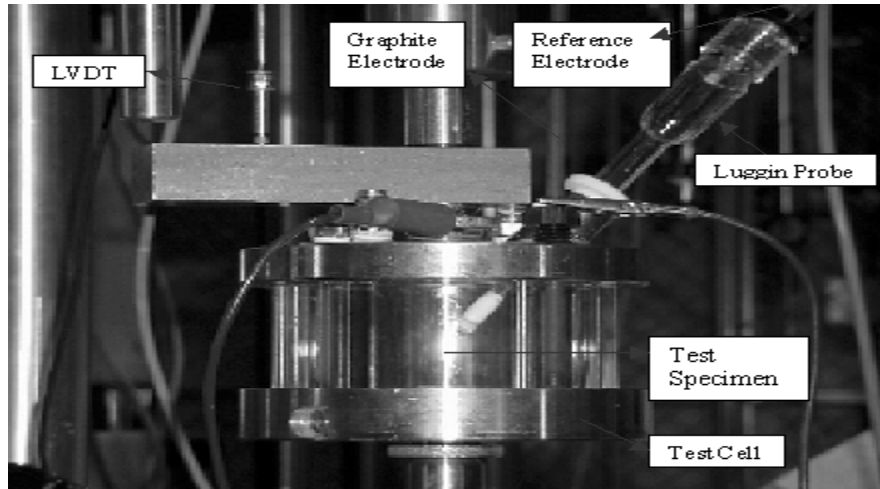


Figure 3.11 SCC test Setup under E_{cont}

3.6. Surface Analyses

The metallurgical properties of an engineering alloy depend on its chemical composition, thermal treatment and their resultant microstructure. The microstructure places an important role in differentiating properties of one alloy versus another. Thus, the evaluation of metallurgical microstructure of a material of interest constitutes a significant step in characterizing the performance of this material, when exposed to a hostile environment under tensile stress. In view of this rationale, it is always customary to evaluate the metallurgical microstructure by optical microscopy at meaningful magnifications. Simultaneously, the characterization of failure, in particular, the extent and morphology of primary and secondary failure by optical microscopy and SEM, respectively, is critical to develop a fundamental understanding on the failure mechanism of a material under certain environmental conditions.

Accordingly, significant emphasis has been placed in this project to characterize the metallurgical microstructure and fractography of Alloy HT-9 using optical microscopy

and SEM, respectively. The detailed analytical procedures are discussed next in the following subsection.

3.6.1. Optical Microscopy

It is very important to ensure that sample preparation was carried out with care to produce high quality and useful micrographs. During the sample preparation, care was taken to ensure that the material was sectioned at a proper location for characterization of a specific feature. The sample was mounted using the right ratio of epoxy and hardener. Steps were taken to ensure that the mounted specimen had the appropriate thickness to prevent rocking during grinding and polishing. The edges of the mounted specimen were rounded to minimize the damage to the grinding and polishing discs.

The mounted specimens were ground with rotating discs of abrasive paper. The grinding procedure involved several stages using a finer paper each time. This was done to remove scratches resulting from the previous coarser paper. The removal of scratches was done by orienting the sample perpendicular to the previous scratches. The polished sample was then washed with deionized water to prevent contamination. Finally, etching was done by using Fry's reagent to reveal the microstructure of Alloy HT-9 using standard etching procedures. Care was taken to ensure that the specimen was not over-etched. The specimen was then immediately washed with deionized water and subsequently dried with acetone and alcohol.

The metallographic evaluations of the mounted specimens were performed by using a Leica optical microscope with a magnification of up to 100X. The optical micrographs showing the microstructure and secondary crack, if any, were obtained in both as-polished and the etched conditions.

3.6.2. Scanning Electron Microscopy

Electron microscope uses a beam of highly energetic electrons to examine objects on a very fine scale. This examination can yield information on topography, morphology, composition and crystallographic information.

A sample of length 1 cm was cut from the tested specimen by using a precision cutter. The sample was then held on a sample holder by using a double-sided carbon tape. The mounted specimens were examined by SEM to determine the morphology of failure in all specimens and cracking along the primary fracture face of the tested tensile specimens.

CHAPTER 4

RESULTS

4.1 Constant-Load SCC Test

The results of SCC testing in neutral and acidic solutions using smooth cylindrical specimens at constant load are shown in Table 4.1. An examination of this table indicates that Alloy HT-9 did not undergo failure in the neutral solution at 30 and 60°C when loaded at an applied stress equivalent to 95% of this material's room temperature YS value. However, failure was observed with this material in the 90°C neutral solution at the same applied stress level. Subsequently, SCC tests were performed in the same solution at 90°C at applied stresses equivalent to 90 and 85% of the material's YS value, showing failures at 86 and 114 hours, respectively. No failures were observed in this environment at 90°C when loaded at 80% of the YS value of this material suggesting that the threshold stress (σ_{th}) for this alloy may range between 80 and 85% of its YS in the 90°C neutral solution, as illustrated in Figure 4.1.

The results of SCC testing in the acidic solution, shown in Table 4.1, indicate that even though no failure was observed at 30°C, Alloy HT-9 exhibited failures in 60 and 90°C when loaded at 95% of this material's YS value. Subsequently, SCC tests were performed in a similar environment at lower applied stresses at 60 and 90°C. The results indicate that failures were observed at both temperatures when loaded at 90 and 85% of the material's YS value. However, no failures were observed at an applied stress

corresponding to 80% of the material's YS value at either testing temperature. These results may suggest that the magnitude of σ_{th} in this environment may range between 80 and 85% of the material's YS value irrespective of the testing temperature. It is, however, interesting to note that the failure time at 90°C was relatively lower compared to that at 60°C, as expected. Graphical representations showing the magnitude of σ_{th} using smooth specimens in the acidic solution at 60 and 90°C are illustrated in Figure 4.2.

Table 4.1 Results of CL SCC Tests using Smooth Specimens

Environment	Applied Stress		Temperature (°C)	TTF (Hours)
	% YS	Stress (ksi)		
Neutral Solution	95	104.5	30	NF
	95	104.5	60	NF
	95	104.5	90	54
	90	99	90	86
	85	93.5	90	114
	80	88	90	NF
Acidic Solution	95	104.5	30	NF
	95	104.5	60	99
	90	99	60	137
	85	93.5	60	172
	80	88	60	NF
	95	104.5	90	51
	90	99	90	79
	85	93.5	90	113
80	88	90	NF	

NF: No Failure

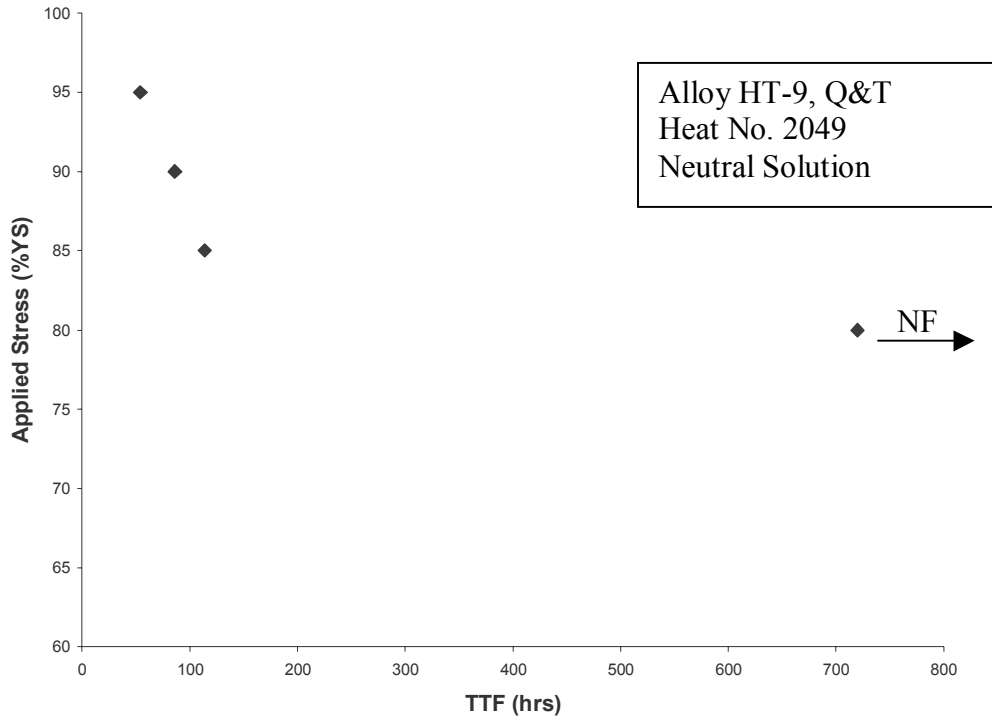


Figure 4.1 Applied Stress vs TTF for Smooth Specimen

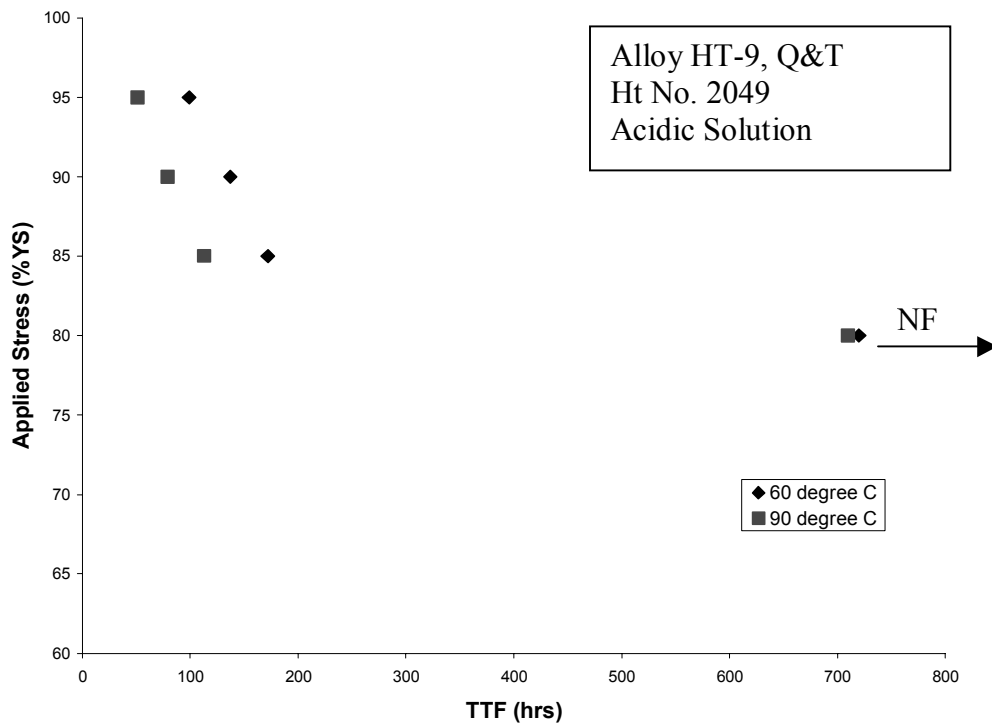


Figure 4.2 Applied Stress vs TTF for Smooth Specimens

The results of SCC testing using notched specimens under constant loading condition in the acidic solution at ambient temperature and 90°C are shown in Table 4.2. As expected, the presence of a notch in the cylindrical specimen reduced the magnitude of σ_{th} to a much lower value. For example, at ambient temperature, the threshold stress was close to 40% of the material's YS value. It should be noted that the notched specimen could not be loaded at stresses above 0.40YS value since the specimen broke during the loading stage. On the other hand, the magnitude of σ_{th} was close to 0.25YS value of the test material at 90°C. The applied stress versus TTF for the notched specimens tested in the 90°C acidic solution is shown in Figure 4.3, providing the magnitude of σ_{th} .

Table 4.2 Results of CL SCC Tests using Notched Specimens

Environment	Applied Stress		Temperature (°C)	TTF
	%YS	Stress (ksi)		Hours
Acidic Solution	40	44	30	NF
	40	44	30	NF
	40	44	30	NF
	40	44	90	21
	40	44	90	20
	40	44	90	18
	35	38.5	90	109
	35	38.5	90	107
	35	38.5	90	100
	30	33	90	240
	30	33	90	233
	30	33	90	256
	25	27.5	90	NF
	25	27.5	90	NF
	25	27.5	90	NF

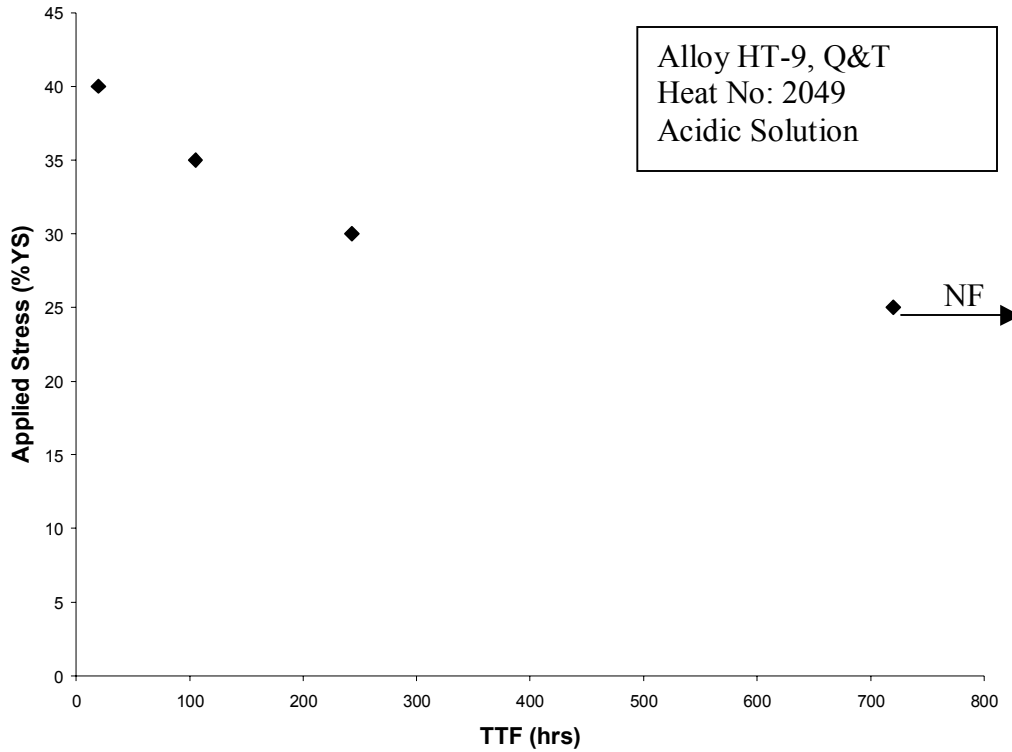


Figure 4.3 Applied Stress vs TTF for Notched specimen

4.2 Slow-Strain Rate SCC Testing

A comparison of the stress-strain diagrams using smooth cylindrical specimens obtained in SSR testing in the neutral and acidic solutions at different temperatures are shown in Figures 4.4 and 4.5, respectively. These figures reveal that the magnitude of strain was gradually reduced with increasing temperature irrespective of the testing environment. The data shown in these two figures are reproduced in Table 4.3, showing the effect of temperature and pH on the true failure stress (σ_f), TTF, %El and %RA, which are conventionally used to characterize the cracking susceptibility of a material of interest when tested by the SSR technique.

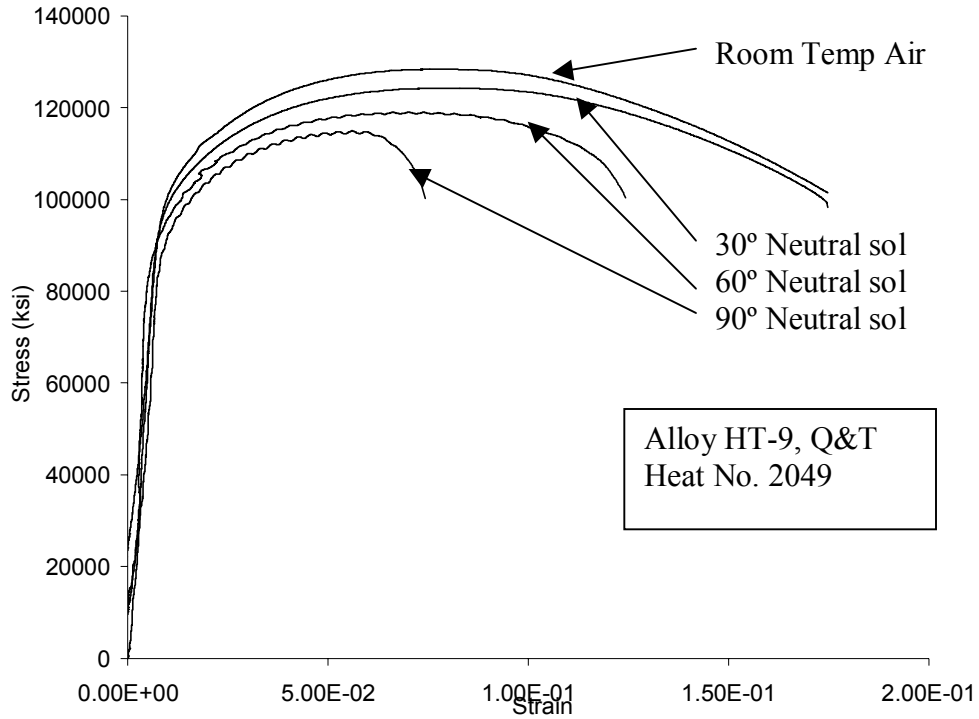


Figure 4.4 Comparison of σ - ϵ Diagrams using Smooth Specimens in Neutral Solution

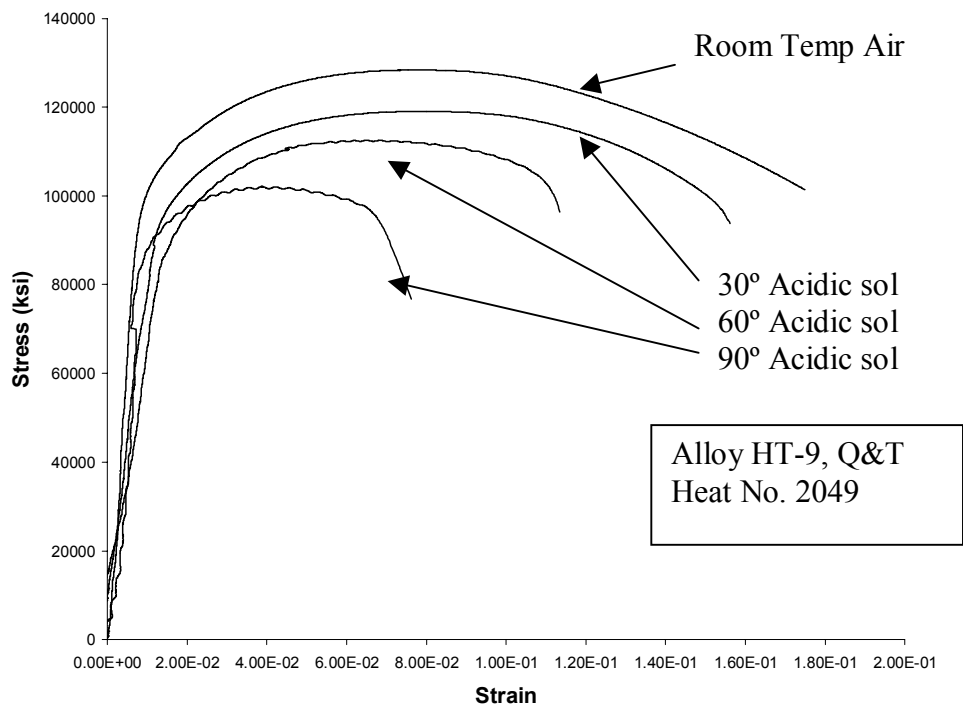


Figure 4.5 Comparison of σ - ϵ Diagrams using Smooth Specimens in Acidic Solution

Table 4.3 SSR Test Results using Smooth Specimens

Environment	Temperature(°C)	%El	%RA	UTS (ksi)	σ_f (ksi)	TTF (hour)
Air	Ambient	21	47.8	130	193	18.8
Neutral Solution	30	19.83	46.3	125	186	18.5
	60	16.5	42	119	172	15.0
	90	12.32	34.83	115	152	10.6
Acidic Solution	30	17.8	44.2	120	170	16.2
	60	14.2	40.19	113	158	13.8
	90	11	34.22	101	118	9.6

An examination of Table 4.3 reveals that the magnitude of σ_f , TTF, %El and %RA was gradually reduced with increasing temperature, showing more pronounced effect in the acidic environment. The difference in value of the actual %El with the strain value in graph is due to compliance of SSR testing machine. The stress-strain ($\sigma - e$) diagrams obtained in neutral and acidic solutions using notched specimens are illustrated in Figures 4.6 and 4.7, respectively, once again showing reduced strains at higher testing temperatures. The magnitude of average σ_f , TTF, %El, %RA determined from these plots are given in Table 4.4, showing a similar trend on the effect of temperature and pH on these parameter, as observed earlier with the smooth specimens. The data presented in this table are the average value of two data point that showed insignificant variation between the two.

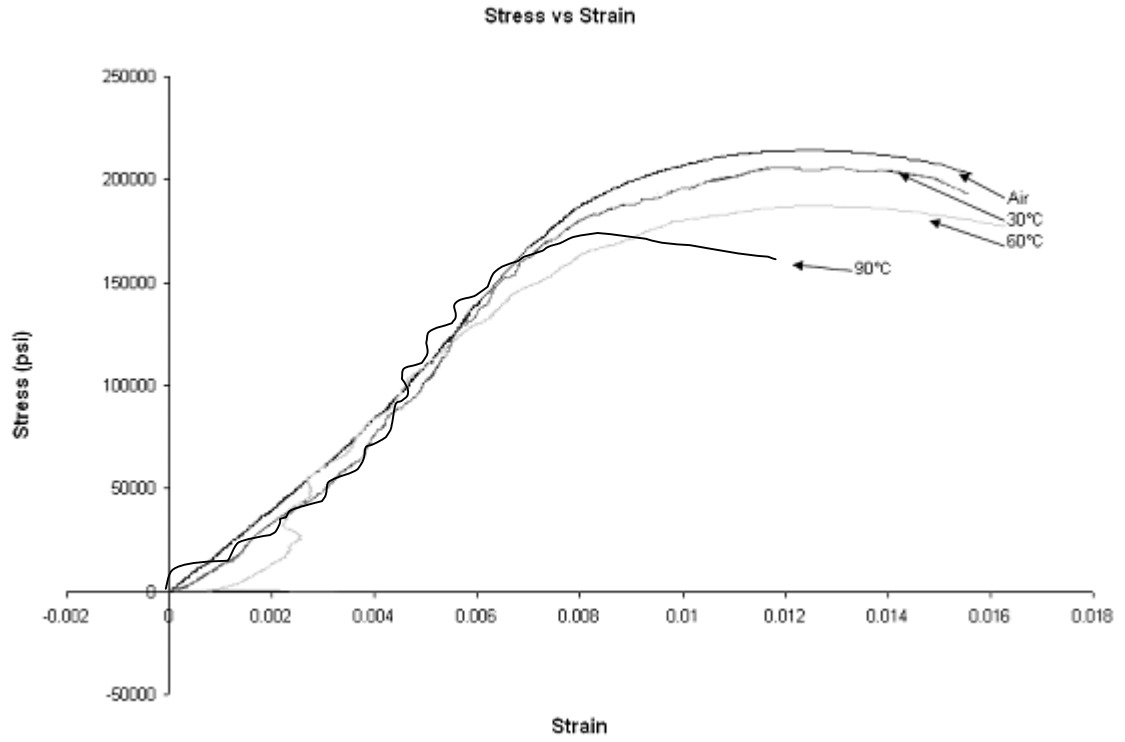


Figure 4.6 Comparison of σ - ϵ Diagrams using Notched Specimens in Neutral Solution

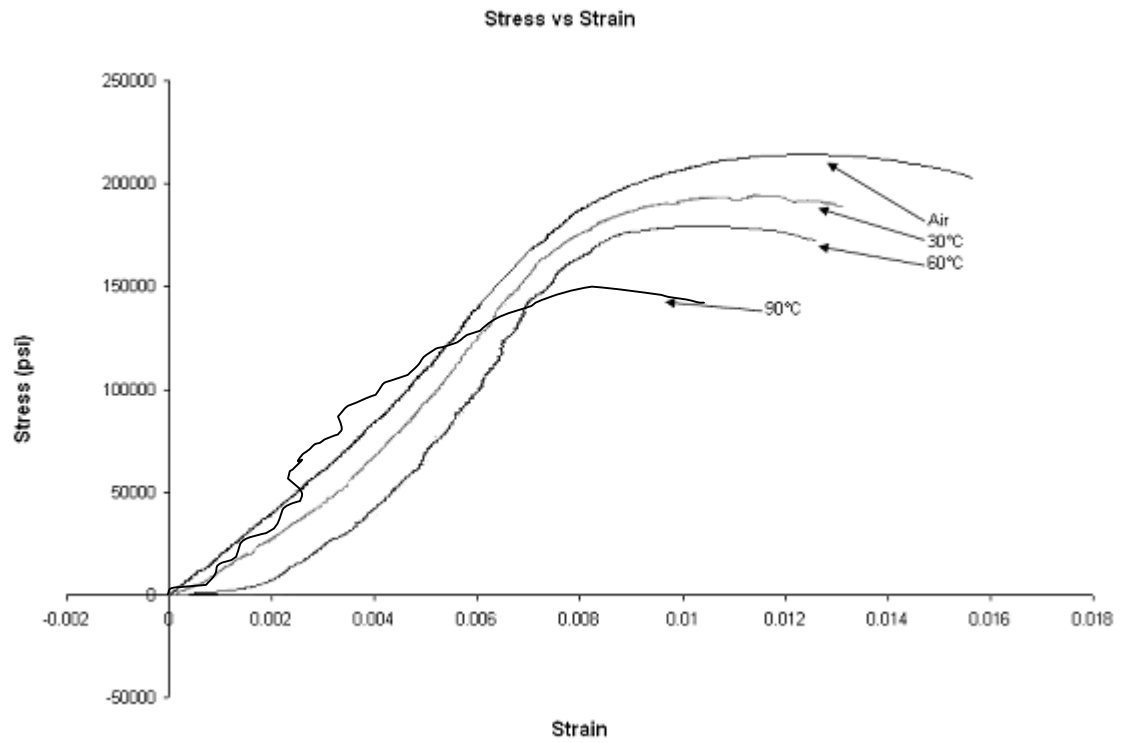


Figure 4.7 Comparison of σ - ϵ Diagrams using Notched Specimens in Acidic Solution

Table 4.4 SSR Test results using Notched Specimens

Environment	Temperature(°C)	%EI	%RA	UTS(Ksi)	σ_f (Ksi)	TTF(hrs)
Air	Ambient	2.45	5.92	215	211	4.4
Neutral Solution	30	1.65	5.62	200	200	4.1
	30	1.45	5.80	208	202	4.3
	60	1.40	5.06	188	190	4.1
	60	1.10	5.10	183	174	3.9
	90	0.95	4.80	174	168	3.7
	90	0.90	4.40	175	164	3.5
Acidic Solution	30	1.40	5.16	195	207	4.3
	30	1.70	5.54	210	195	4.1
	60	1.25	4.98	180	174	3.8
	60	1.20	4.30	175	181	3.8
	90	0.75	3.82	158	155	3.6
	90	0.55	3.68	160	158	3.6

The results of SSR testing using smooth and notched cylindrical specimens, shown in Tables 4.3 and 4.4, respectively are graphically reproduced in Figures 4.8 through 4.11, showing the effects of temperature, pH and specimen geometry on σ_f , TTF, %EI, %RA. An examination of these figures clearly indicate that all these parameters were reduced in either testing environment at elevated temperatures showing more pronounced effect in the acidic solution. The presence of a notch significantly reduced the TTF, %EI and %RA. However, the magnitude of σ_f increased in the presence of a notched due to the relatively smaller cross-sectional area at the root of the notch that also produced a large mechanical constraint in the vicinity of the notch.

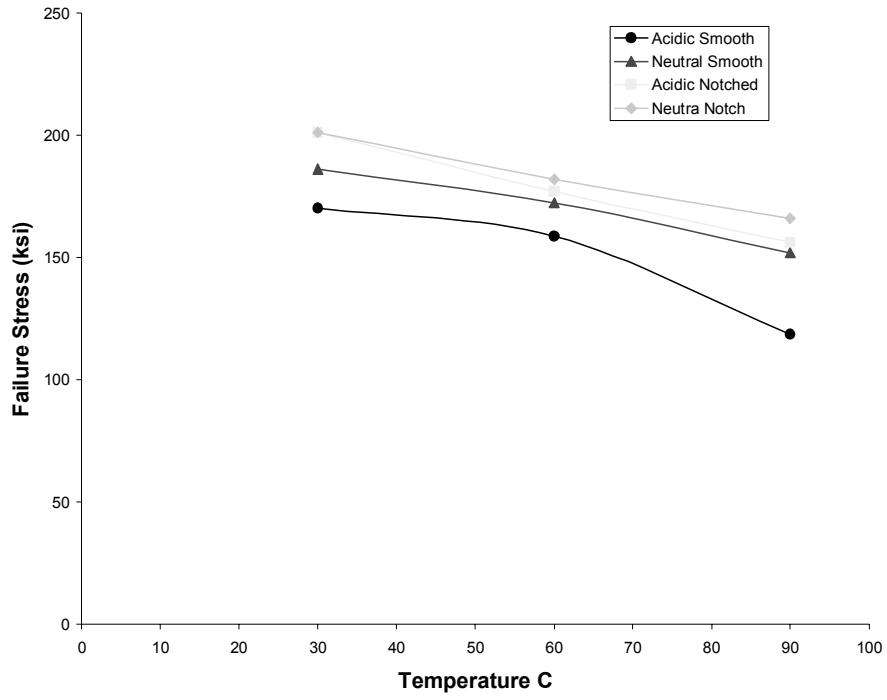


Figure 4.8 Temperature vs Failure Stress

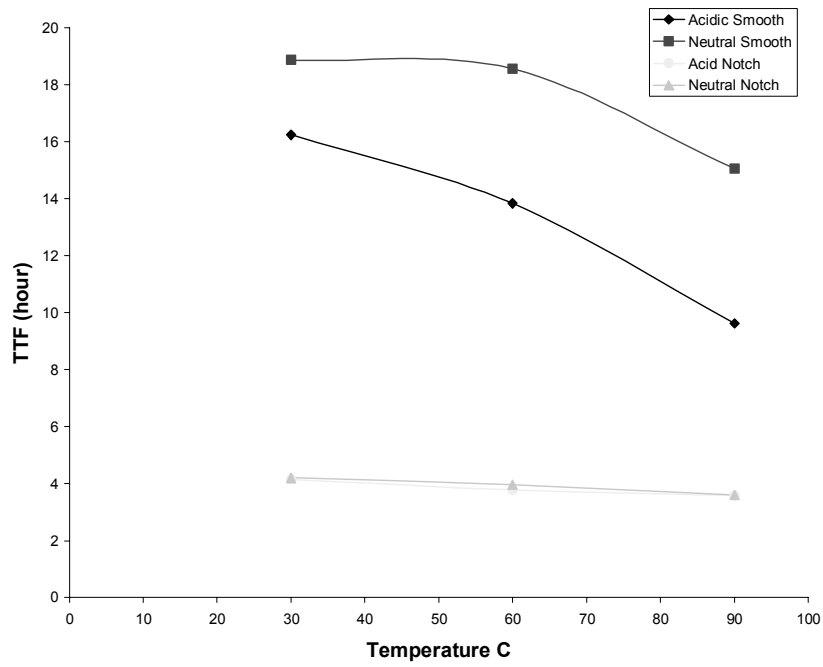


Figure 4.9 Temperature vs TTF

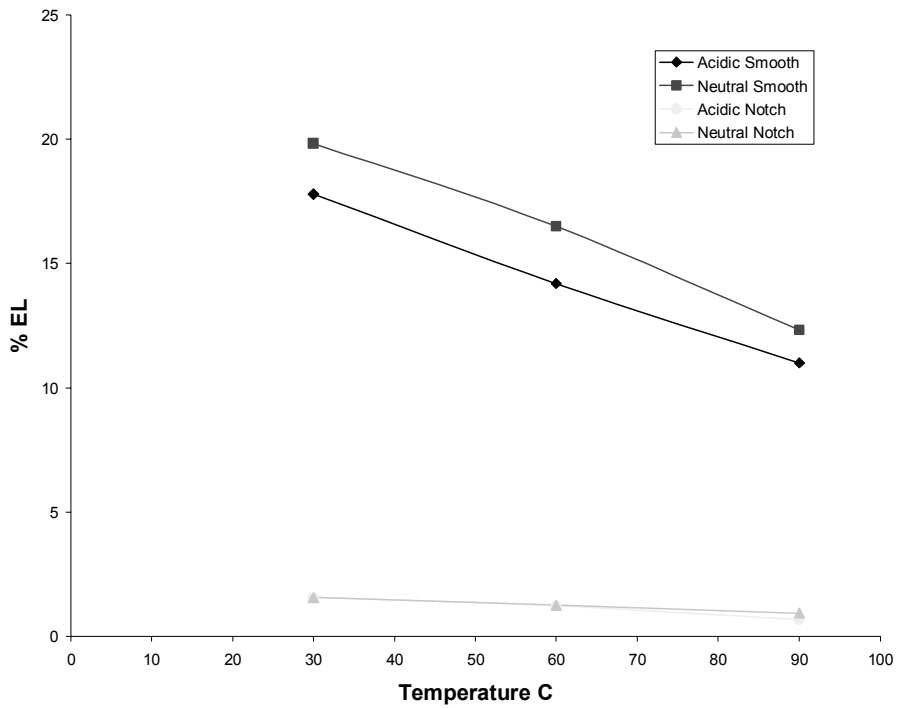


Figure 4.10 Temperature vs %EI

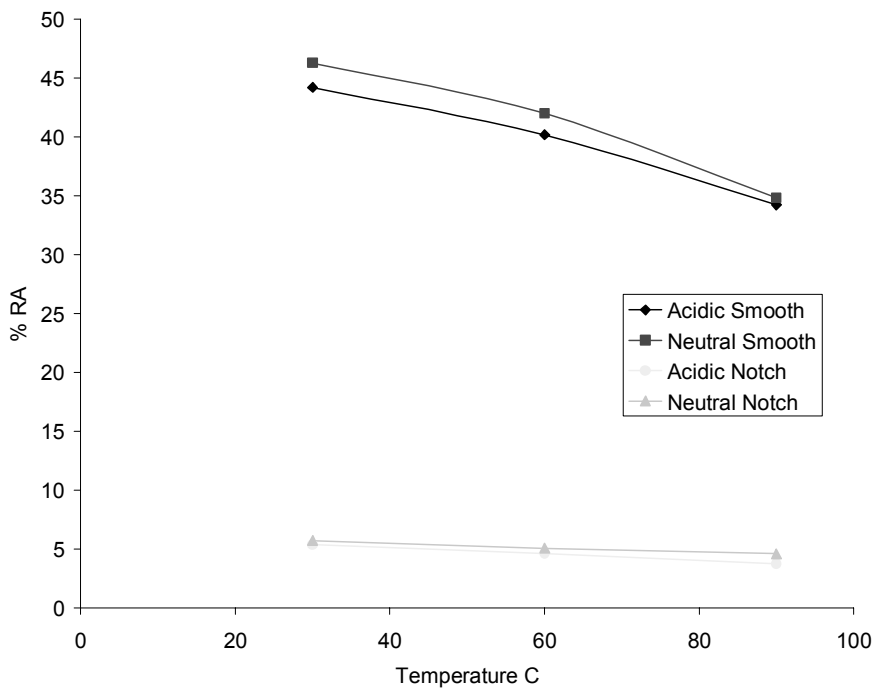


Figure 4.11 Temperature vs %RA

4.3 SCC Testing using Self-Loaded Specimens

As indicated earlier in this thesis, an evaluation of embrittlement of Alloy HT-9 in the presence of molten LBE was of prime importance. However, the desired SCC testing using self loaded specimens such as C-ring and U-bend could not be accommodated at LANL due to some unavailability of facilities. SCC testing incorporating similar types of specimens was performed at UNLV using an aqueous acidic environment at ambient temperature, 50 and 100°C using either a desiccator (room temperature) or an autoclave (elevated temperatures).

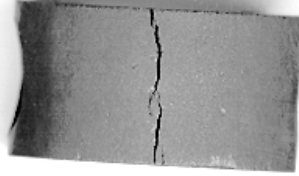
One of the drawbacks of using C-ring and U-bend specimens to evaluate the SCC behaviors of a material of interest is that the final load/stress experienced by either type of specimen cannot be controlled. In case of C-ring specimen, the desired deflection of the ring was given by changing its outer diameter through application of a stress by means of a bolt, based on the YS of the test material using Equation 3.6, shown in the previous section.^[20] However, in case of the U-bend specimen, the initial stress or load cannot be estimated. Thus, an arbitrary deflection between the two arms was given to produce stress in this type of specimen. Nevertheless, the evaluation of SCC susceptibility using C-ring or U-bend specimen is based on the tensile stress experienced by the outer layer of either type of specimen, while exposed to an aggressive environment such as an acidic solution used in this investigation. The C-ring specimens tested in this investigation were loaded by applying stresses on their outer layer that corresponded to 95 and 98% of the YS value of Alloy HT-9.

The results of SCC testing using C-ring specimens of Alloy HT-9 indicate that cracks were observed in the acidic solution both at 50 and 100°C at applied stresses

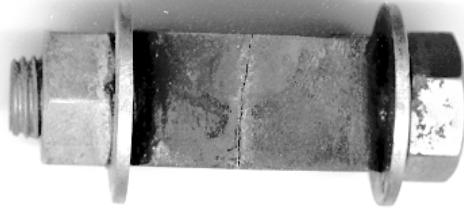
corresponding to 95 and 98% of this material's yield strength value. However, the time to initiate cracking in the 50°C acidic solution was significantly higher (7 weeks) compared to that (2 days) in the 100°C acidic solution. The appearances of the C-ring specimens tested at both temperatures are illustrated in Figure 4.12. None of the U-bend specimens of Alloy HT-9 showed any cracking in the tested environment at either testing temperature. However, they showed some parallel degradation marks (crack-like indications), as shown in Figure 4.13, indicating that cracks could have been initiated in these specimens provided they were exposed for longer durations.



(a) 100°C, $\sigma_a = 0.95Y_S$, 2 Days

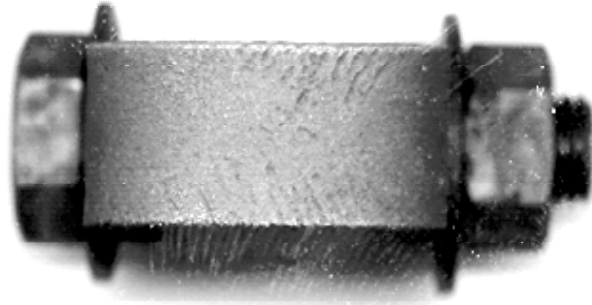


(b) 50°C, $\sigma_a = 0.98Y_S$, 7 weeks



(c) 100°C, $\sigma_a = 0.98Y_S$, 2 Days

Figure 4.12 Appearance of C-ring Specimens Tested in Acidic Solution



(a) Top View



(b) Front View

Figure 4.13 Appearance of U-bend Specimen in Acidic Solution

4.4 SCC Testing at controlled potential

The susceptibility of Alloy HT-9 to hydrogen-induced cracking was determined by applying cathodic electrochemical potential (E_{cont}) to the spot-welded cylindrical specimen while loaded in tension by the SSR technique. The magnitude of E_{cont} was based on the corrosion potential (E_{corr}) determined by a previous investigator [22] at UNLV. The results, shown in Figures 4.14 and 4.15 indicate that the magnitude of strain was reduced at ambient temperature and 90°C due to the application of E_{cont} , indicating reduced ductility.

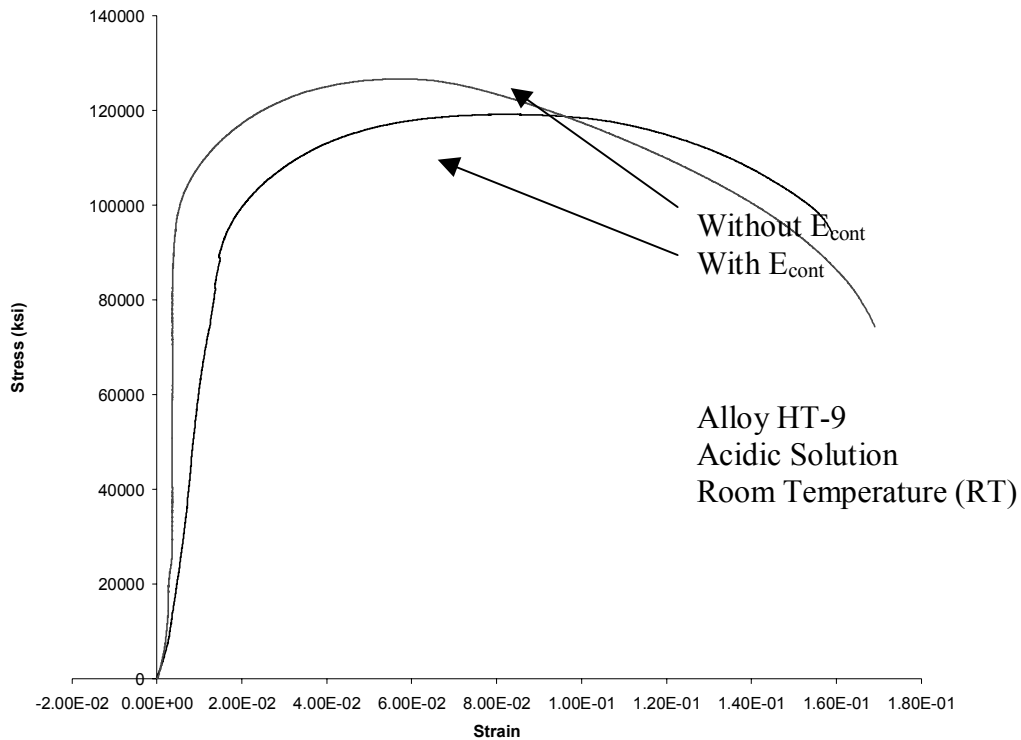


Figure 4.14 Stress-Strain Diagrams with and without E_{cont} at RT

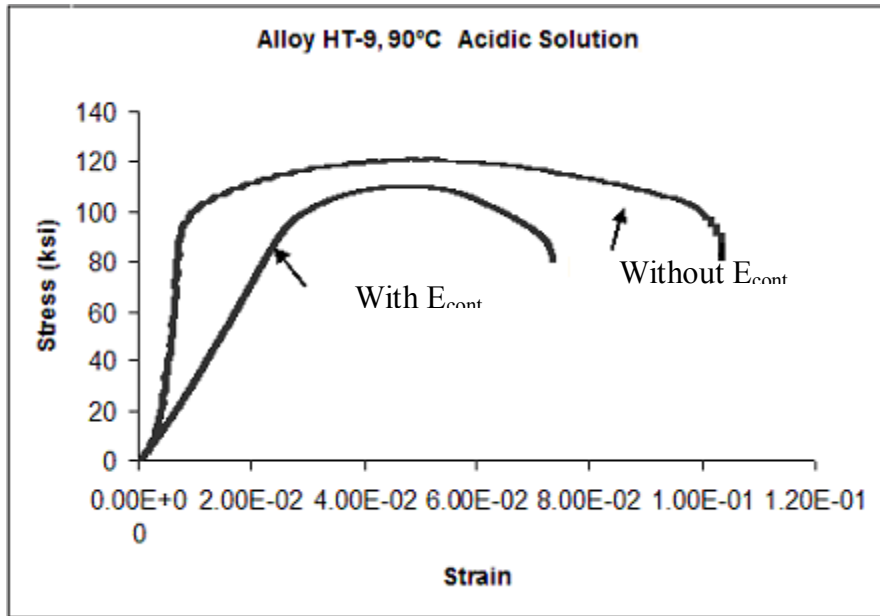


Figure 4.15 Stress-Strain Diagrams with and without E_{cont} ^[22] at 90°C

4.5 Results of Micrograph Evaluation

4.5.1 Optical Microscopy:

Figure 4.16 illustrates the metallurgical microstructure of Alloy HT-9 following quenching and tempering. Examination of this figure confirms that fully-tempered and fine-grained martensitic microstructure was developed in this alloy. As shown earlier, ductility was significantly reduced in specimens loaded in tension while exposed to a 90°C acidic solution. An examination of the tested specimens in this environment revealed secondary cracks along the gauge section of the broken specimen, as shown in Figure 4.17, as determined by optical microscopy. An optical micrograph of a failed C-ring specimen of Alloy HT-9 is shown in Figure 4.18, illustrating the extent of cracking on its outer surface.

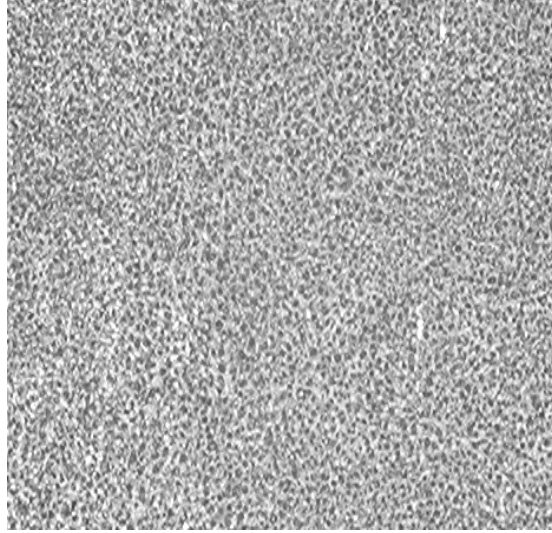


Figure 4.16 Optical Micrograph of in Q&T condition
Etched in Fry's Reagent, 10X

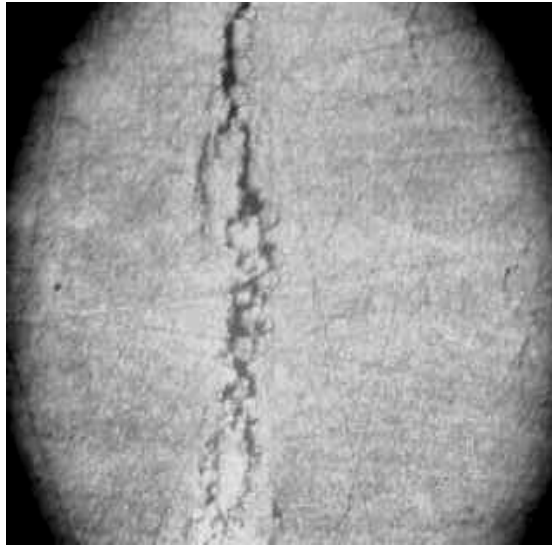


Figure 4.17 Secondary Cracks Determined by Optical Microscopy
Etched in Fry's Reagent, 10X

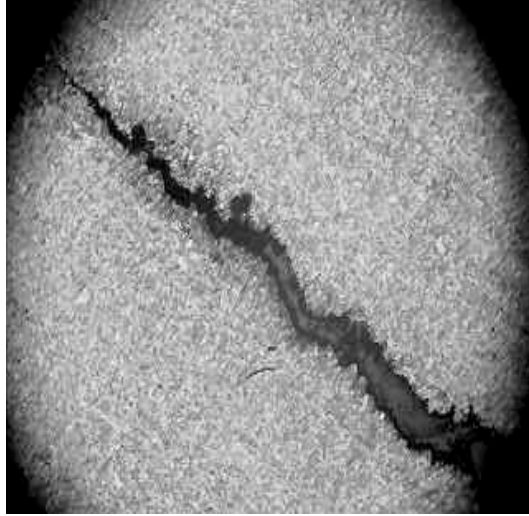
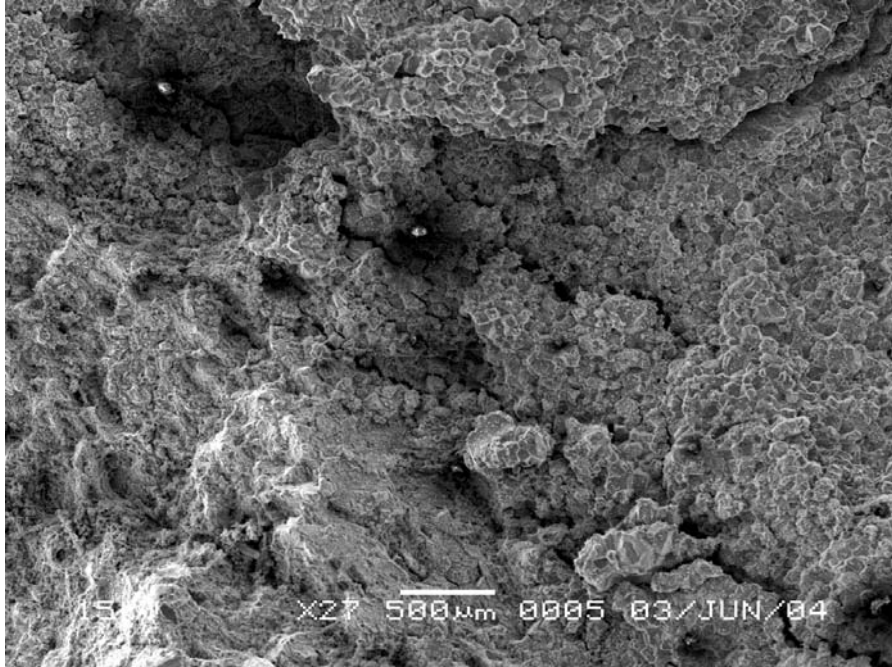


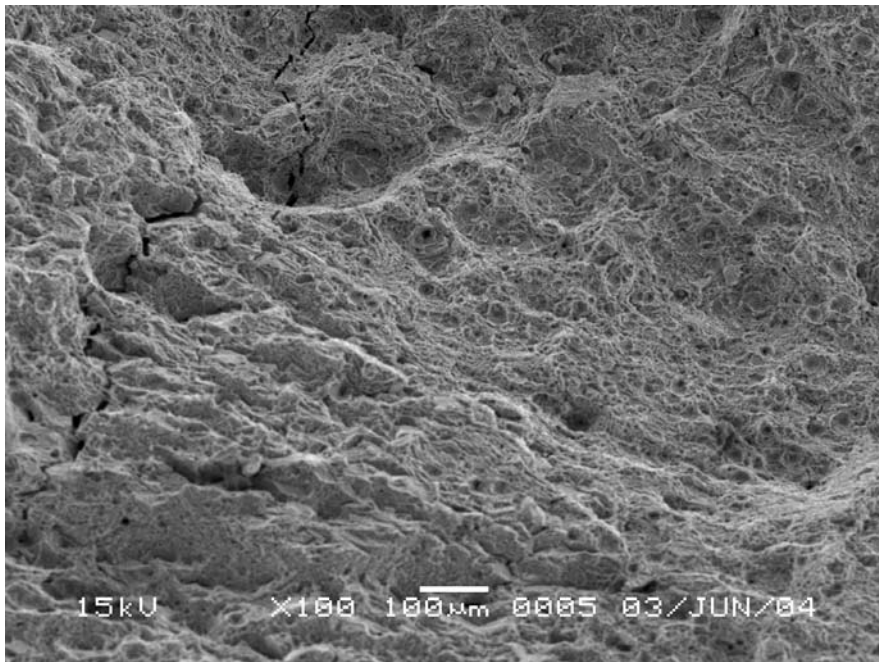
Figure 4.18 Optical Micrograph of Failed C-ring Specimen
Etched in Fry's Reagent, 10X

4.5.2 Scanning Electron Microscopy:

The results of fractographic evaluation of the primary fracture faces of the cylindrical specimens of Alloy HT-9, tested in both neutral and acidic solutions, are shown in Figure 4.19. An examination of these micrographs reveals that both intergranular and transgranular cracks were developed in the tested specimens irrespective of test solution. However, dimpled microstructure, indicative of ductile failures, were also observed in these specimens. An evaluation of the fractured C-ring specimens by SEM revealed intergranular failure, as illustrated in Figure 4.20.



(a) 90°C Neutral Environment



(b) 90°C Acidic Environment

Figure 4.19 SEM Micrographs of the Primary Fracture Face of Alloy HT-9

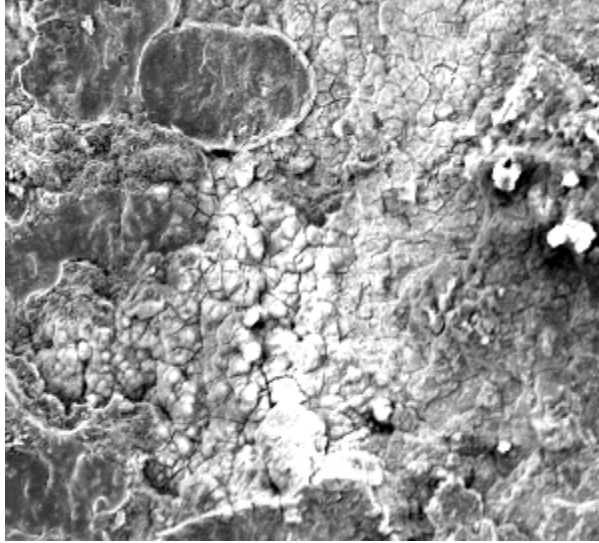


Figure 4.20 Intergranular Brittle Failure in C-ring Specimen in 100°C Acidic Solution

CHAPTER 5

DISCUSSION

As described in previous sections, martensitic Alloy HT-9 has been evaluated for its resistance to SCC and HE in neutral and acidic environments at ambient and elevated temperatures using constant-load and slow-strain-rate testing techniques. Since SCC testing involving self-loaded specimens in LBE could not be performed at LANL, testing was performed at UNLV using C-ring and U-bend specimens in aqueous solutions. An effort was also made to study the effect of hydrogen on the cracking susceptibility of Alloy HT-9 by applying cathodic electrochemical potential to the test specimen under SSR condition. Microstructural evaluation and characterization of secondary cracks along the gage section of the tensile specimens were performed by optical microscopy. Further, the extent and morphology of failure at the primary fracture face of the tested tensile specimens were determined by SEM. A brief, but relevant discussion on different topics related to this investigation is presented in the next few subsections.

5.1 Constant-Load SCC testing

The results of SCC testing involving smooth tensile specimens at constant load in either environment revealed failures at applied stresses equivalent to 95, 90 and 85% of the material's YS value at 90°C. However, no failures were observed in this alloy when tested in both environments at 90°C at applied stress equivalent to 80% of its YS value,

suggesting a threshold stress (σ_{th}) in the vicinity of 80 to 85% of this material's YS value. It is, however, interesting to note that the TTF in the acidic solution was relatively lower compared to that in the neutral solution. The presence of a notch substantially reduced the magnitude of σ_{th} in both environments. ^[21] A similar effect of notch on the cracking susceptibility of martensitic stainless steel was observed by other investigators. ^[22]

5.2 Slow-Strain-Rate SCC Testing

The results of SSR testing using both smooth and notched specimens indicate that, in general, the magnitude of strain was reduced with increasing temperature. This effect was more pronounced in the acidic solution. These data also indicate that parameters such as %EI, %RA, TTF and σ_f were gradually reduced with increasing temperature, once again showing more pronounced effect in the acidic environment. This effect, which may be attributed to the synergistic effect of acidic pH and higher testing temperature, has also been cited by other investigators. ^[23] The presence of a notch further reduced the magnitude of these parameters, as expected. ^[24] It is, however, interesting to note that the magnitude of σ_f was enhanced in the notched specimen due to the reduced cross-sectional area at the root of the notch and mechanical constraint resulting from the stress concentration effect.

5.3 Self-Loaded SCC Testing

The results of SCC testing in the acidic solution using C-ring specimen of Alloy HT-9 indicated that this material may experience cracking when tested at an applied stress equivalent to 95 and 98% of the material's YS value at elevated temperatures. However,

the cracking susceptibility was more pronounced at 100°C, compared to that at 50°C, irrespective of the applied stress level. On the other hand, the U-bend specimens did not exhibit any cracking, except for the fact that some crack-like indications were observed on their outer surfaces. This data may indicate that the cracking could have been initiated in these specimens if they were tested for longer durations.

5.4 SCC testing under E_{cont}

The results of a limited number of SCC tests involving smooth specimens of Alloy HT-9 in the acidic solution at controlled cathodic potential indicate that the ductility parameters, TTF and σ_f were reduced to some extent. This phenomenon may be attributed to the generation of more hydrogen ions (H^+) in the acidic solution due to cathodic charging. The resultant data, showing a reduction in ductility, matches observations made by other investigators. [22, 25]

5.5 Microscopic Evaluation

Metallographic evaluations by optical microscopy revealed typical metallurgical microstructure of a quenched and tempered martensitic alloy, and branched secondary cracks along the gage section of the tested cylindrical specimens. The SEM micrographs revealed both ductile and brittle failures in cylindrical specimens. Ductile failures were characterized by dimpled microstructure. [26, 27] On the other hand, brittle failures were indicated by intergranular and transgranular cracks at the primary fracture face of the tested specimens, irrespective of the testing solution. [26, 27] SEM micrographs of the

cracked C-ring specimen showed a combination of ductile and intergranular brittle failure when loaded under a tensile stress along its outer surface.

CHAPTER 6

SUMMARY AND CONCLUSIONS

The susceptibility of Alloy HT-9, a candidate target structural material, to stress corrosion cracking (SCC) and hydrogen embrittlement (HE) has been evaluated in neutral and acidic solutions at ambient and elevated temperatures. The cracking susceptibility has been determined by using constant-load, slow-strain-rate (SSR) and self-loaded testing methods. The susceptibility to cracking in the presence of hydrogen has been evaluated by applying cathodic (negative) electrochemical potential to the specimen tested under a SSR condition. The extent and morphology of failure along the primary fracture face of the tested specimens have been evaluated by scanning electron microscopy (SEM). Metallographic evaluations have been performed by optical microscopy. The significant conclusions drawn from this investigation are summarized below.

- Alloy HT-9 suffered from failures in both neutral and acidic solutions at elevated temperatures under constant loading conditions. The magnitude of the threshold stress (σ_{th}) for cracking was reduced in both environments due to the presence of a notch in the tensile specimens.
- The extent of ductility in terms of %El and %RA, as well as TTF and σ_f were gradually reduced with increasing temperature in the SSR testing. This effect of temperature was more pronounced in the acidic solution. The presence of notch, however, increased the magnitude of σ_f .

- C-ring specimens of Alloy HT-9 exhibited through-all cracking from the convex surface to the concave surface of the specimen in 50 and 100°C acidic solution when tested at applied stresses equivalent to 95 and 98% of this material's yield strength value. Some crack-like indications were also observed with the U-bend specimens at 100°C in a similar testing environment.
- Application of a -1000mV potential to the tensile specimen caused reduction in ductility parameters, σ_f and TTF indicating a detrimental effect of hydrogen on the cracking susceptibility of Alloy HT-9 in the 90°C acidic solution.
- Branched secondary cracks were observed along the gage section of the tensile specimen, when evaluated by optical microscopy.
- Fractographic evaluations of the primary fracture face by SEM revealed a combination of ductile failure characterized by dimpled microstructure, and intergranular/transgranular brittle failure.
- An analysis of the overall data involving alloys EP-823, HT-9 and 422 in the advanced fuel cycle initiative (AFCI) research program clearly indicates that Alloy EP-823 would be the most viable target structural material in view of its superior metallurgical and corrosion properties due to the presence of higher silicon content.

CHAPTER 7

FUTURE WORK

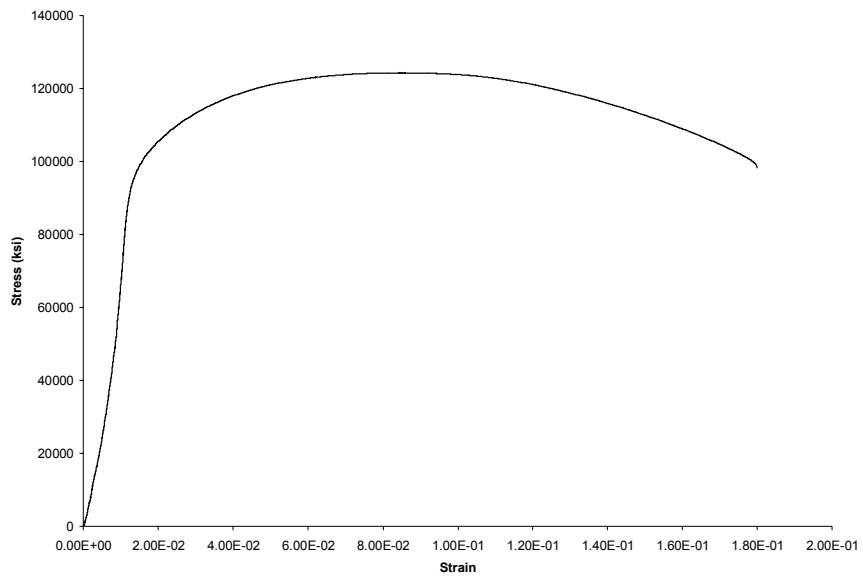
Since SCC testing could not be performed involving Alloy HT-9 in the presence of molten LBE, it is suggested that a comprehensive metallurgical and corrosion study be performed either at UNLV or Los Alamos National Laboratory in future using molten LBE as the testing environment.

APPENDIX
SLOW STRAIN RATE DATA

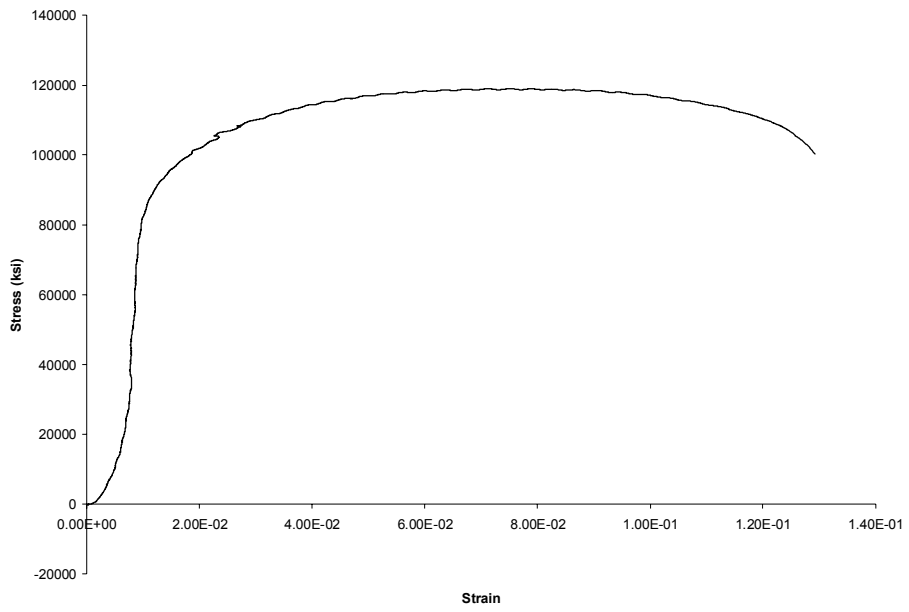
1. Smooth Tensile Specimen

a. Neutral

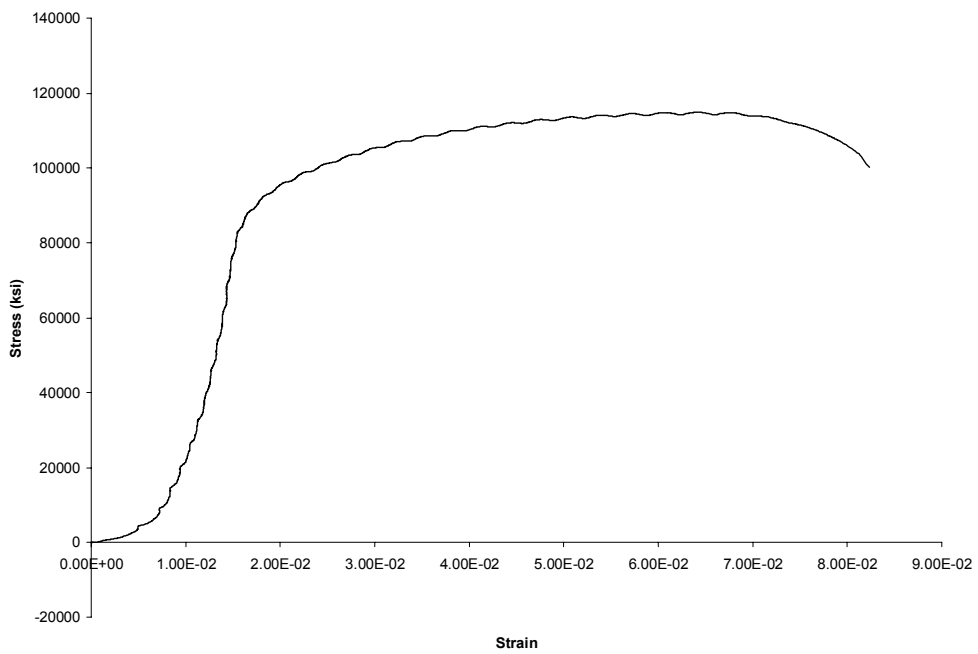
i. 30 °C



ii. 60 °C

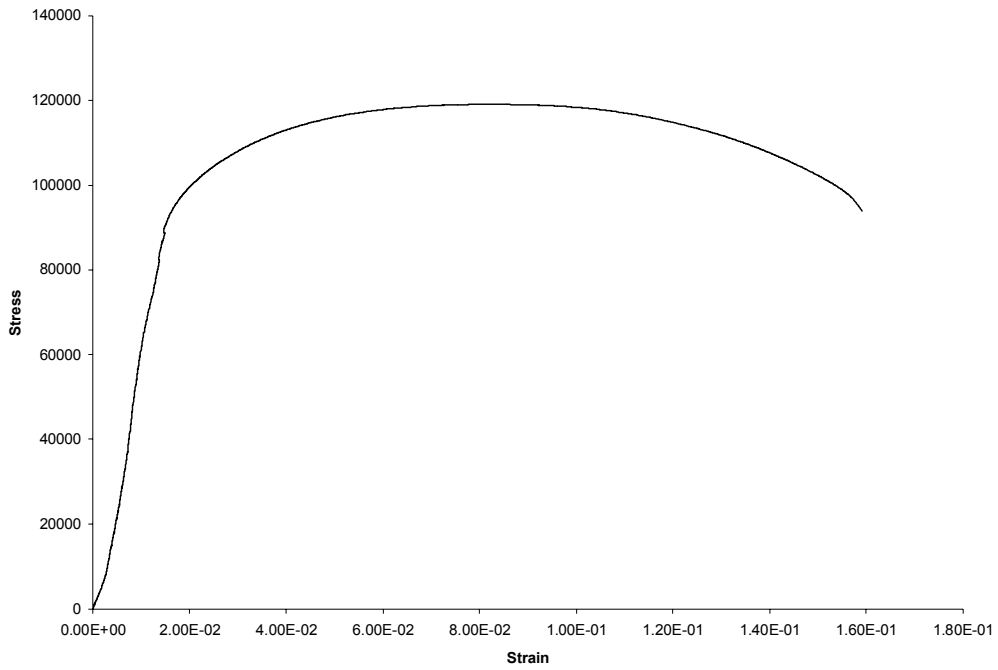


iii. 90 °C

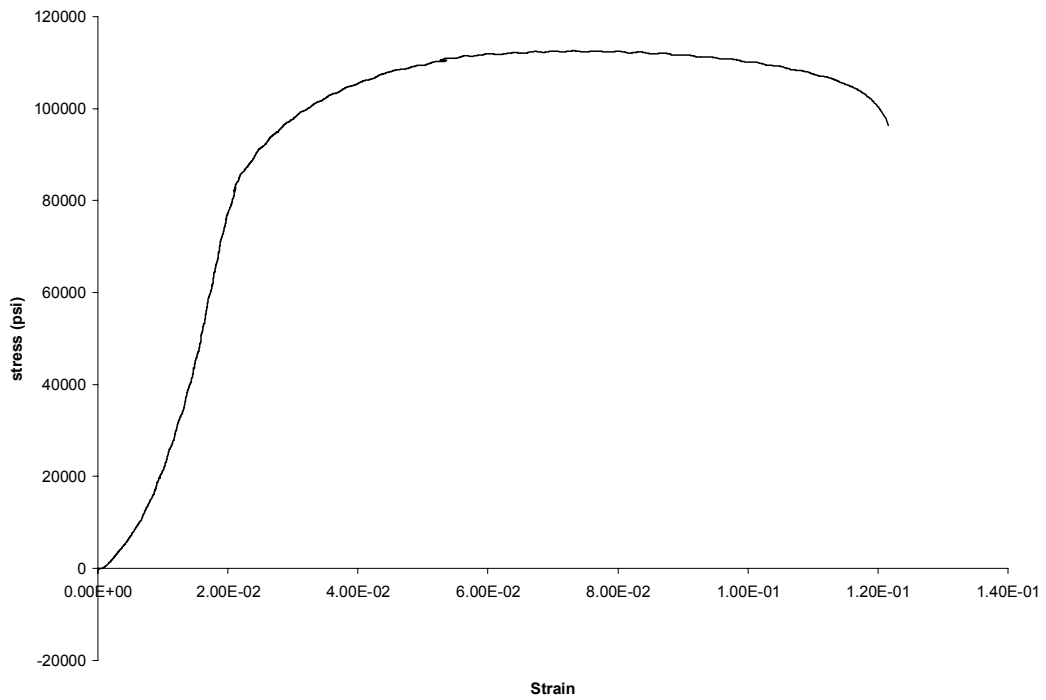


b. Acidic Solution

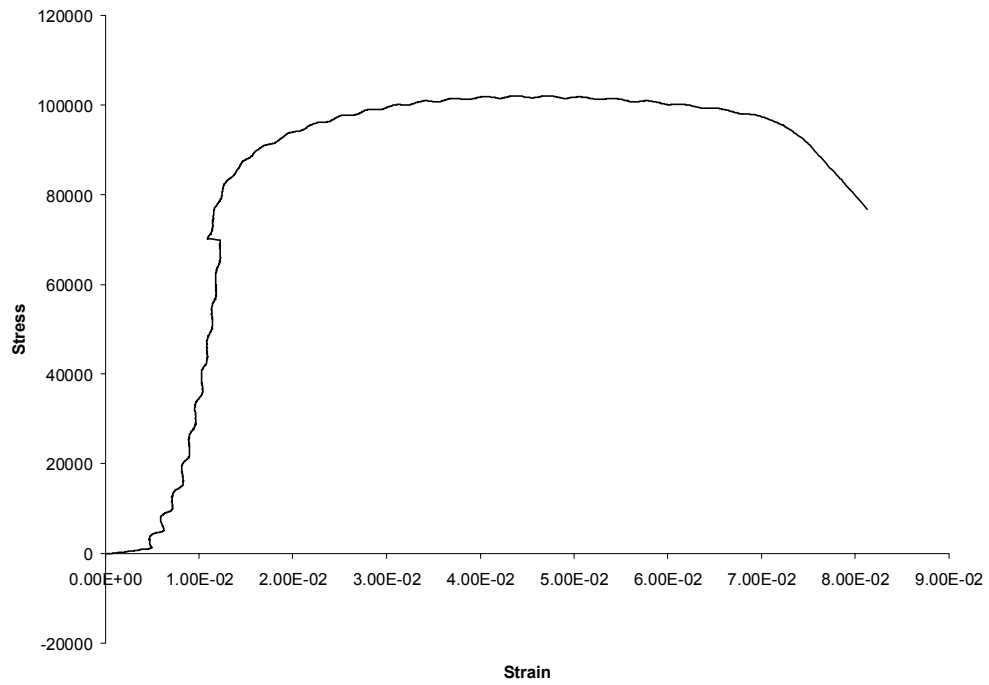
i. 30 °C



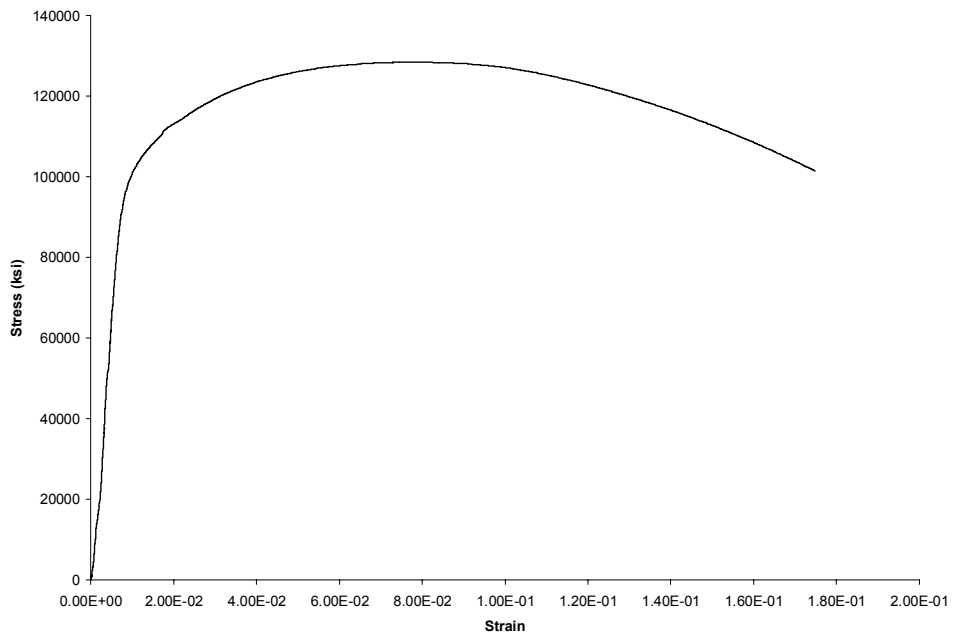
ii. 60° C



iii. 90° C



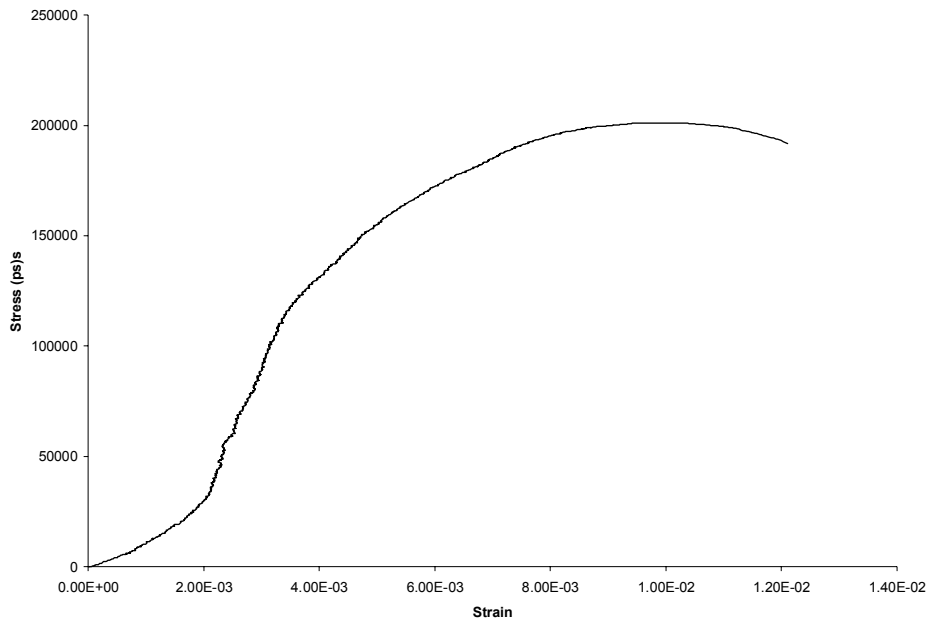
3. AIR



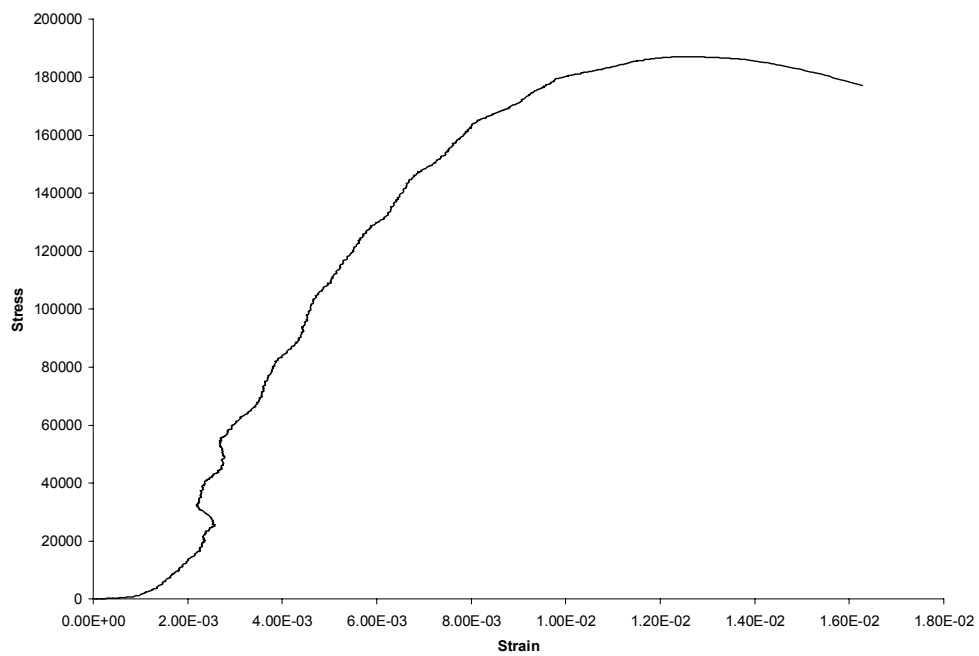
2. Notched Results

a. Neutral

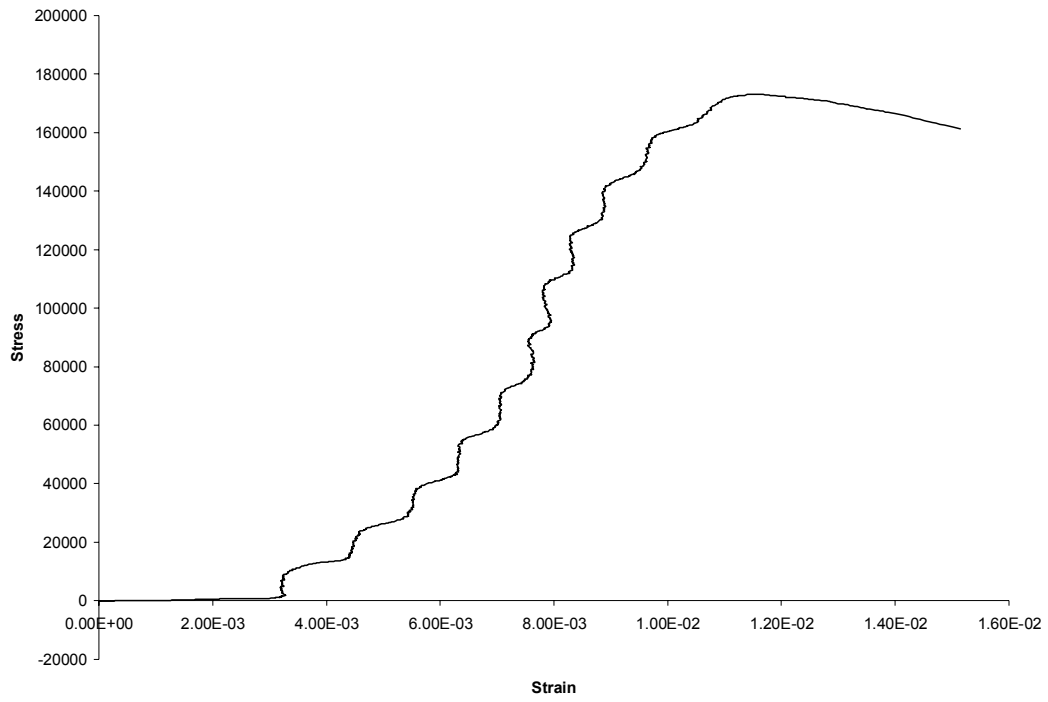
i. 30° C



ii. 60° C

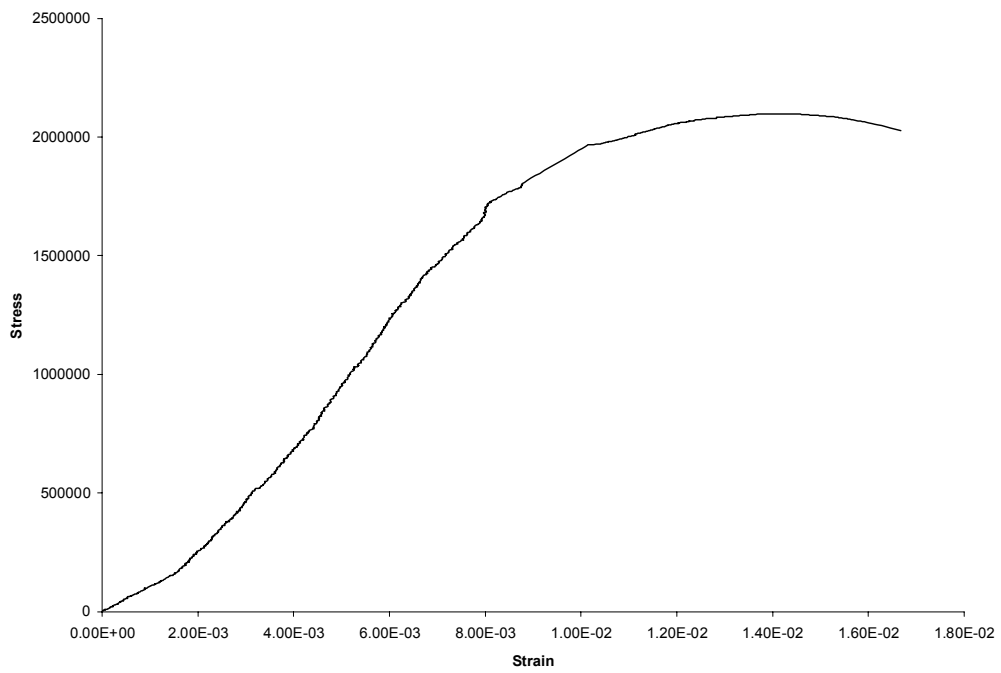


iii. 90° C

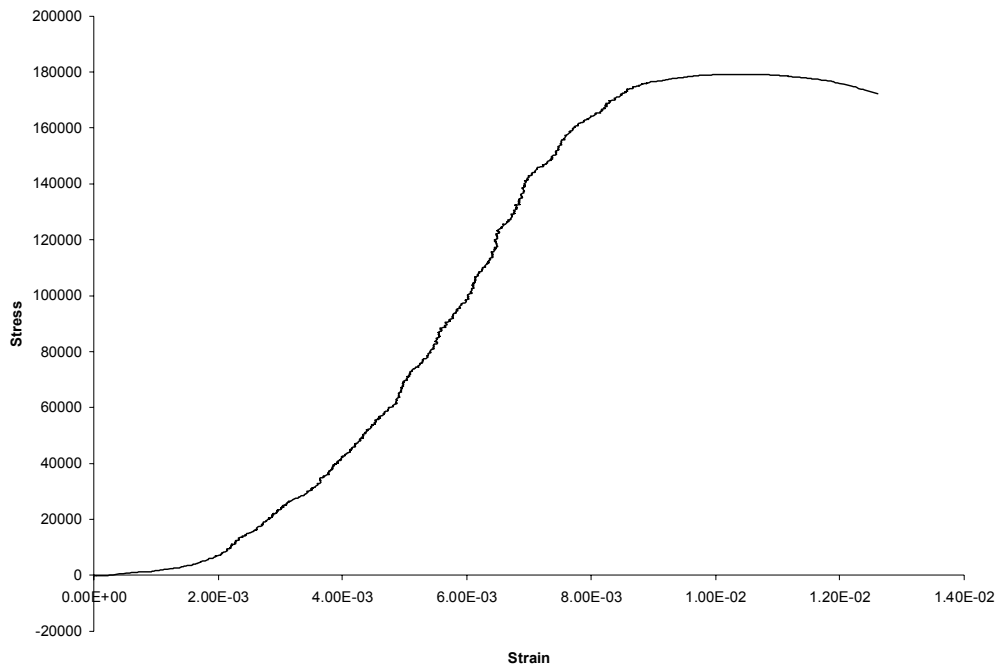


b. Acidic

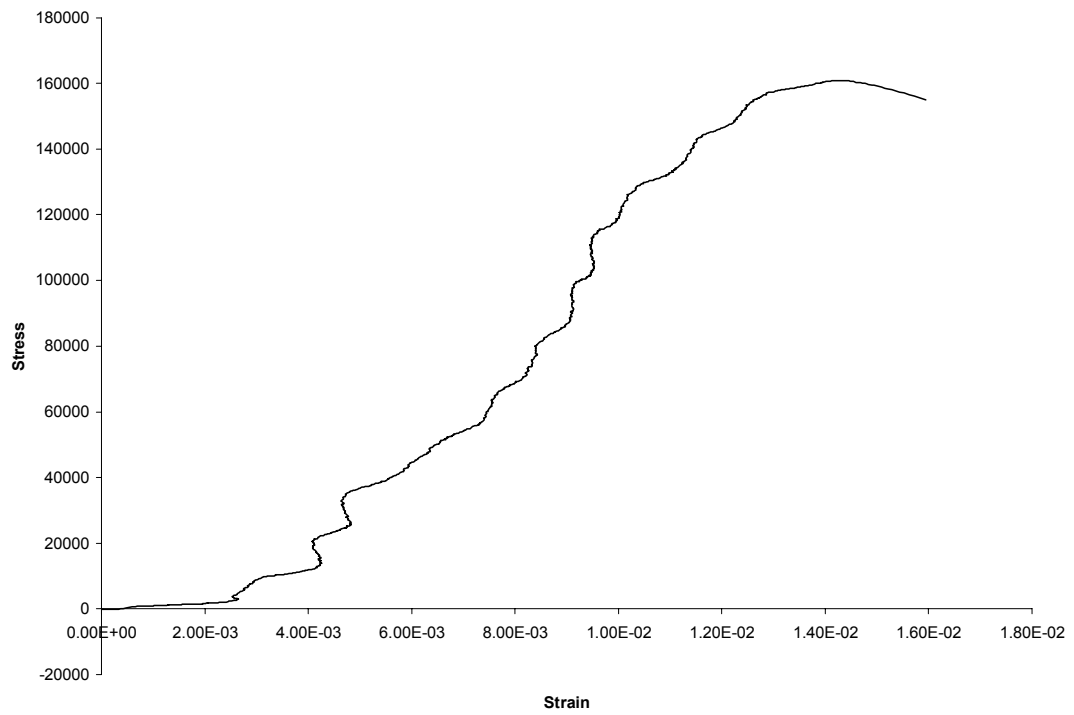
i. 30° C



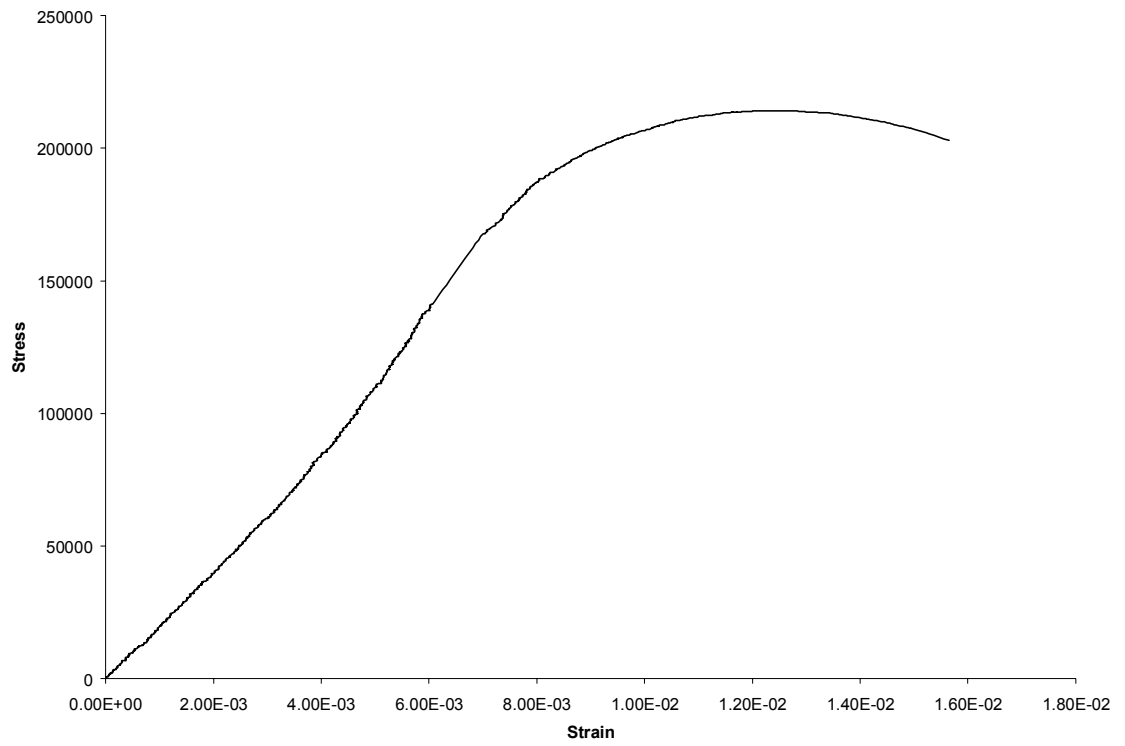
ii. 60° C



iii. 90° C



c. AIR



BIBLIOGRAPHY

1. F. Venneri, et al., "Disposition of Nuclear Waste using Subcritical Accelerator-Driven Systems: Technology Choices and Implementation Scenarios," *Nuclear Technology*, Vol. 132, No. 1, pp. 15 (2000)
2. P. Jung, C. Liu, J. Chen, "Retention of Implanted Hydrogen and Helium in Martensitic Stainless Steels and their Effects on Mechanical Properties." *Journal of Nuclear Materials*, 296, pp. 165-173 (2001)
3. H. Rauh and H. Ullmaier, "Hydrogen Concentrations near Cracks in Target Materials for High-Power Spallation Neutron Sources," *Journal of Nuclear Materials*, Elsevier Science, 295, pp. 109 (2001)
4. Y. Kurata, et al., "Excellent corrosion resistance of 18Cr-20Ni-5Si steel in liquid Pb-Bi," *Journal of Nuclear Materials*, 325, pp. 217-222 (2004)
5. A.L. Johnson, et al., "Spectroscopic and Microscopic Investigation of the Corrosion of 316/316L Stainless Steel by Lead-Bismuth Eutectic (LBE) at Elevated Temperatures: Importance of Surface Preparation," Accepted for *Journal of Nuclear Materials*
6. George E. Dieter., *Mechanical Metallurgy*, 1998, p. 496-500
7. Mars G. Fontana., *Corrosion Engineering*, 1987, p. 137-152
8. Nelson HG. Hydrogen embrittlement. In: Briant CL, Banerji SK, editors. *Treatise on materials science and technology*, vol. 25. New York: Academic Press, 1983. p. 275-359.

9. D. H Mesa, A. Toro, A. Sinatora, A.P Tschiptschin, The Effect of testing temperature on corrosion-erosion resistance of martensitic stainless steels.
10. H.E Boyer (Ed.), Metals Handbook, vol. 10, American Society for Metals, Metals Park, Ohio, 1975, pp. 217-218.
11. Kimura, A. and H. Matsui, "Neutron Irradiation Effects on the Microstructure of Low-Activation Ferritic Alloys," J. Nucl. Mater. 212-w215, 1994,701.
12. Lucas , G.e., Odette, G.R., Maiti, R., Sheckherd, J. w., "Tensile Properties of irradiated Pressure Vessel Steels," ASTM-STP-956, American Society for Testing and Materials, 1987, p379-385
13. A.J. GRIFFITHS and A.TURNBULL: Proc. Conf on Structural Materials in Marine Environments', London, UK, May 1994, the Institute of Materials, 324-329.
14. ASTM Designation: E 8-89b, Standard Test Methods of Tension Testing of Metallic materials
15. March, J.L., Ruprecht, W. J., and Reed, George, "Machining of Notched Tension Specimens," ASTM Bulletin, ASTBA, Am.Soc.Testing Mats., No.244 1960, pp.52-55
16. Cortest, Incorporated Website (<http://www.cortest.com>)
17. A. K. Roy, et al., "Cracking of Titanium Alloys under Cathodic Applied Potential," Micron, Vol 32, No 2, Elsevier Science, Feb 2001, Pg 211-218
18. ASTM Designation: G38-01, Standard Practice for Making and Using C-Ring Stress-Corrosion Test Specimens.
19. ASTM Designation: G30-97, Standard Practice for Making and Using U-Bend Stress-Corrosion Test Specimens.

20. N.Eliaz, A.Shachar, B.Tal, D.Eliezer, "Charecteristics of hydrogen embrittlement, stress corrosion cracking and tempered martensitic embrittlement in high-strength steels," *Engineering Failure Analysis* 9, 2002, Pg 167-184
21. Ajit K. Roy, *Ramprashad Prabhakaran*, "Stress Corrosion Cracking of Type 422 Stainless Steel for Transmutation Applications," *Proceedings of International Youth Nuclear Congress (IYNC) 2004*, Paper No 119
22. Sudheer Sama, "Embrittlement and Localized Corrosion in Alloy HT-9," M.S.Thesis, UNLV, August 2004
23. Ajit K. Roy, *Ramprashad Prabhakaran*, et al., "Stress Corrosion Cracking of Nuclear Transmutation Structural Materials," *Materials Performance, NACE International*, September 2004, Vol. 43, No. 9, pp. 52-56
24. *Ramprashad Prabhakaran*, Ajit K. Roy, Mohammad K. Hossain, Sudheer Sama, "The Effect of Environmental and Mechanical Variables on Stress Corrosion Cracking of Martensitic Stainless Steels for Transmutation Applications," *Proceedings of The 12th International Conference on Nuclear Engineering (ICONE12)*, Paper No. 49399, April 25-29, 2004.
25. Birnbaum HK. Mechanisms of hydrogen related fracture of metals. In: Moody NR, Thompson AW, editors. *Proceedings of the fourth International Conference on the effect of Hydrogen on the behavior of Materials*. Wyoming, 1990: Warrandale: TMS, 1989. p. 639-60.
26. Ajit K. Roy, *Ramprashad Prabhakaran*, Mohammad K. Hossain, Sudheer Sama, Brendan J. O'Toole, "Environment-Induced Degradation of Spallation Target Materials,"

American Nuclear Society (ANS) Meeting, AccApp'03, Paper No. 79416, June 1-5, 2003.

27. Ramprashad Prabhakaran, "Environmental Effects on a Candidate Structural Material for Transmutation Application," ANS Student Conference 2004, April 1-3, 2004, Madison, WI.

VITA

Graduate College
University of Nevada, Las Vegas

Venkataramakrishnan Selvaraj

Local Address:

4248 Cottage Circle, Apt # 1
Las Vegas, NV 89119

Permanent Address:

1700E 13th Street, Apt # 8GE
Cleveland, OH 44114

Degree:

Bachelor of Engineering, Mechanical Engineering, 2002
University of Madras, Chennai, India

Special Honors and Awards:

Member, American Nuclear Society
Member, American Society of Testing Methods

Publications/Presentations:

Venkataramakrishnan Selvaraj, Phani K. Gudipati, "Cracking of Target Structural Materials in Different Environments," American Nuclear Society (ANS) Annual Student Conference, April 1-April 3, 2004, University of Wisconsin, Madison

Ajit K. Roy, Venkataramakrishnan Selvaraj, Phani K. Gudipati, "Environment Degradation of Martensitic Stainless Steel for Transmutation Applications," Material Science and Technology (MS&T), October, 2004, New Orleans, Louisiana

Ajit K. Roy, Ramprashad Prabhakaran, Mohammad K. Hossain, Sudheer Sama, Venkataramakrishnan Selvaraj, Phani K. Gudipati, "Environmental Effects on Materials For Nuclear Applications," Materials Science & Technology (MS&T) 2003, November 9-12, 2003, Chicago, Illinois

Ajit K. Roy, Ramprashad Prabhakaran, Mohammad K. Hossain, Sudheer Sama, Venkataramakrishnan Selvaraj, Phani K. Gudipati, "Effect of Environmental Variables on Cracking of Martensitic Stainless Steels under Different Loading Conditions," American Nuclear Society (ANS) Meeting-Global 2003, Paper No. 87869, November 16-20, 2003, New Orleans, Louisiana

Ajit K. Roy, Ramprashad Prabhakaran, Mohammad K. Hossain, Sudheer Sama, Venkataramakrishnan Selvaraj, Phani K. Gudipati, "Cracking of Target Materials under Cathodic Applied Potential," The National Association of Corrosion Engineers (NACE) International-Corrosion 2004, Paper No. 4559, March 28-April 1, 2004, New Orleans, Louisiana

Thesis Title: ENVIRONMENT ASSISTED CRACKING OF TARGET STRUCTURAL MATERIALS UNDER DIFFERENT LOADING CONDITIONS

Thesis Examination Committee:

Chairperson, Dr. Ajit K. Roy, Ph. D.

Committee Member, Dr. Anthony E. Hechanova, Ph. D.

Committee Member, Dr. Brendan J. O'Toole, Ph. D.

Graduate College Representative, Dr. Rama Venkat, Ph. D.